Wang *et al. Energy Mater* 2024;4:400080
DOI: 10.20517/energymater.2024.57

Energy Materials

Review

Open Access

Small components play a big role - fillers in composite solid-state electrolytes for lithium metal batteries

Zhixuan Wang, Hang Yang, Suo Li, Hao Tong, Wenhao Xu, Yangmingyue Zhao, Libo Li*

School of Materials Science and Chemical Engineering, Harbin University of Science and Technology, Harbin 150080, Heilongjiang, China.

***Correspondence to:** Prof./Dr. Libo Li, School of Materials Science and Chemical Engineering, Harbin University of Science and Technology, No. 52 Xuefu Road, Nangang District, Harbin 150080, Heilongjiang, China. E-mail: lilibo@hrbustu.edu.cn

How to cite this article: Wang Z, Yang H, Li S, Tong H, Xu W, Zhao Y, Li L. Small components play a big role - fillers in composite solid-state electrolytes for lithium metal batteries. *Energy Mater* 2024;4:400080. https://dx.doi.org/10.20517/energymater.2024.57

Received: 31 May 2024 **First Decision:** 5 Aug 2024 **Revised:** 10 Sep 2024 **Accepted:** 30 Sep 2024 **Published:** 13 Dec 2024

Academic Editor: Jiaqi Huang **Copy Editor:** Fangling Lan **Production Editor:** Fangling Lan

Abstract

Lithium metal batteries (LMBs), the energy conversion and storage technologies that have been thoroughly investigated, are utilized in various areas. Most current commercial LMBs use liquid electrolytes, but their safety cannot be guaranteed. In contrast, all-solid-state LMBs with solid-state electrolytes (SSEs) are regarded as next-generation energy storage systems owing to their enhanced safety. In the examination of SSEs, the benefits of composite SSEs (CSSEs) are particularly prominent. CSSEs relying on multiphase composites have better flexibility to tailor electrolyte performance based on demand and, thus, the design of components. Based on existing research presentations, we herein review the development of CSSEs. Firstly, the essential components of CSSEs are introduced, focusing on explaining the transport channel of Li ions within the polymer matrix and the impact of various fillers on this channel. The key performance parameters of CSSEs are described in detail. Subsequently, the fillers in CSSEs are meticulously classified; the critical roles played by different fillers in the polymer matrix are clarified, and the hotspots of current research are summarized. Furthermore, the prevalent structural design methodologies in CSSEs are examined, and the impact of various structures on battery performance is elucidated. Finally, the current problems of CSSEs and the future development prospects are summarized. This review is significant because it provides ideas for the design of CSSEs and contributes to the development of all-solid-state LMBs to realize their wide application.

Keywords: Composite solid-state electrolytes, lithium-ion transport channel, all-solid-state lithium metal batteries, structural design

INTRODUCTION

The advancement of energy storage systems featuring high energy density and enhanced safety is crucial for the continued utilization of mobile electronic gadgets and electric vehicles[1-4]. Lithium metal batteries (LMBs) are regarded as the most effective and efficient energy storage and conversion devices due to their remarkable energy density, prolonged cycle life, and lightweight characteristics[5-7]. With the continuous development and application of LMBs, the performance requirements for LMBs are also increasing. Currently, the most commonly utilized LMBs predominantly rely on liquid electrolytes[8-10]. The liquid electrolyte exhibits high ionic conductivity and superior electrode surface wettability; however, it is frequently plagued by issues, such as inadequate thermal stability, low ion selectivity, and subpar safety[11-13]. Conversely, all-solid-state LMBs (ASSLMBs) utilizing solid-state electrolytes (SSEs) exhibit enhanced safety and prolonged electrochemical and thermal stability, presenting viable solutions to the challenges associated with LMBs[14,15]. Consequently, research on SSEs has exhibited a significant increase in recent years and has become a notable trend in the progression of LMBs[16].

SSEs can be classified into two main categories: ceramic SSEs (CSEs) and polymer SSEs (PSEs)[17,18]. With most of the former being lithium-containing oxides, phosphate and sulfides, such as $Li_{0.33}La_{0.56}TiO_3$ (LLTO) with a perovskite-type structure, $Li_{1.3}Al_{0.3}Ti_{1.7}(PO_4)_3$ (LATP) with a NASICON-type structure, $Li_7La_3Zr_2O_{12}$ (LLZO) with a garnet-type structure, and $Li_{10}GeP_2S_{12}$ (LGPS), a crystalline sulfide[19-21]. Sulfide electrolyte-based LMBs have high safety and energy density, but the poor instability between lithium metal and sulfides and the sensitivity of sulfides to water limit their application[22]. Perovskite and garnet structured oxide electrolytes, together with NASICON structured phosphate electrolytes, demonstrate elevated ionic conductivity, varying from 10^{-4} to 10^{-3} S cm^{-1} at room temperature, and remarkable stability. Due to the rigidity of CSEs, they cannot be in close contact with the electrodes, which generates a large interfacial impedance hindering the transport of Li ions[23,24]. Moreover, certain CSEs may exhibit adverse side reactions at the electrode/electrolyte interface, with the byproducts of these reactions potentially increasing interfacial resistance, thereby degrading battery performance. These limitations have significantly restricted the broader utilization of CSEs[25,26].

The latter type of SSEs is generally composed of organic polymers, including polyvinylidene fluoride (PVDF), polyacrylonitrile (PAN), polyethylene oxide (PEO), *etc.*, as the matrix, and some lithium salts, such as $LiClO_4$ and lithium bis(trifluoromethyl sulfonyl)imide (LiTFSI), as the standard composition[27,28]. The primary advantage of polymer electrolytes is their excellent flexibility, which facilitates intimate contact with the electrode interface, hence minimizing interfacial resistance, and their ease of processing and manufacturing; other advantages also make the polymer electrolyte stronger and more competitive. Nonetheless, polymer electrolytes exhibit significant limitations, such as their comparatively low ionic conductivity at room temperature (between 10^{-6} and 10^{-5} S cm^{-1}) and insufficient thermal stability. Additionally, the mechanical properties of polymer electrolyte films are subpar, making them susceptible to puncture by lithium dendrites. This limitation has become a crucial factor impeding their advancement[29,30]. Research on composite SSEs (CSSEs) including inorganic-organic multiphase composites is progressively developing to address the challenges associated with the use of CSEs or PSEs.

At present, CSSEs are mainly composed of polymers, lithium salts, and fillers. As a key component of ASSLMBs, CSSEs, represented by China, Japan, South Korea, and the United States, have all listed ASSLMBs technology as a key development field, and its research and development has become one of the hot spots in the global science and technology competition[31]. Numerous firms focused on solid-state battery technology have been established or financed, including ProLogium, Automotive Cells Company, Welion, and Quantum Scape. The predominant research trend focuses on addressing the established issues

of CSSEs, including low ionic conductivity, limited electrochemical windows, and inadequate electrode/electrolyte interface compatibility. The main solution is to design the components and structure of CSSEs to achieve improved performance. For example, Li *et al.* designed an electrolyte and applied it to the $LiFePO_4$ (LFP) cathode to enhance the electrode/electrolyte interface issue, thus successfully augmenting the cycle stability of the battery[32]. Still, most of the focus has been on the enhancement of ionic conductivity only, and there has yet to be a systematic summary of the specific roles of different types of fillers in polymers and their effects on properties other than ionic conductivity. Fillers can establish a conductive layer of Li ions at the interface between the electrolyte and the electrode. This layer effectively mitigates the contact resistance to facilitate the transport of Li ions across the interface[33]. Furthermore, the conductive layer on the cathode side prevents direct contact between the electrode and the electrolyte, limiting electrolyte breakdown. The conductive coating on the anode side facilitates the homogeneous deposition of lithium ions and suppresses the formation of lithium dendrites[34,35]. A thorough comprehension of the function of fillers facilitates the customization of CSSEs to diverse requirements; thus, it is crucial to delineate the unique roles of various electrolyte types in polymers. Figure 1 summarizes the advantages and disadvantages of different electrolyte materials and several design approaches for CSSEs.

This review provides a comprehensive examination of the essential functions of fillers in CSSEs. The increase in ionic conductivity observed in polymers when fillers are added is mainly due to the decrease in crystallinity. Additionally, we have provided a detailed overview of how various components in CSSEs facilitate the transport of Li ions and discussed the significance of each key performance indicator. Moreover, we have conducted an extensive review of recent research, specifically focusing on the investigation of different categories of fillers and their unique functions as emerging substances in CSSEs. Furthermore, this review analyzes the relationship between filler and polymer matrix interfaces, including an assessment of filler concentration, size, and morphology to elucidate the formation of lithium-ion transport channels at the polymer-filler interface. Lastly, we have also discussed the various crystal phases, vacancies, and compositions within active fillers to provide microscopic insight into the process of lithium-ion migration.

LITHIUM-ION TRANSPORT AND KEY PARAMETERS IN CSSES

Construction of lithium-ion channels of CSSEs

CSSEs are often formed by including additional inorganic fillers into the PSEs. These fillers may be split into inert fillers that insulate Li ions and active fillers that can conduct Li ions. This chapter will describe the role of each component in CSSEs and the general lithium-ion transport channels.

Lithium-ion channels in polymer electrolytes

The polymer matrix is a crucial component in CSSEs. The lithium-ion transport channel of the polymer chain should first be fully understood to facilitate a better understanding of how CSSEs work. A multitude of polar groups on the polymer chain can coordinate with lithium, facilitating the adsorption of Li ions onto the polymer chain. When the polymer chain undergoes linkage movement, Li ions will migrate from the coordination site where it was initially located to other adjacent coordination sites[47]. Furthermore, when the temperature of the polymer matrix attains its glass transition temperature (T_g), it facilitates the movement of chain segments within the polymer, hence accelerating lithium-ion migration, which is the predominant mechanism of lithium-ion transport in polymers[48]. The presence of space between the polymer chains facilitates the migration of Li ions, allowing them to hop across different segments of the chains. The interplay of short-range migration and long-range motion of the polymer chains facilitates the transport of Li ions in the PSEs[49,50], as shown in Figure 2A.

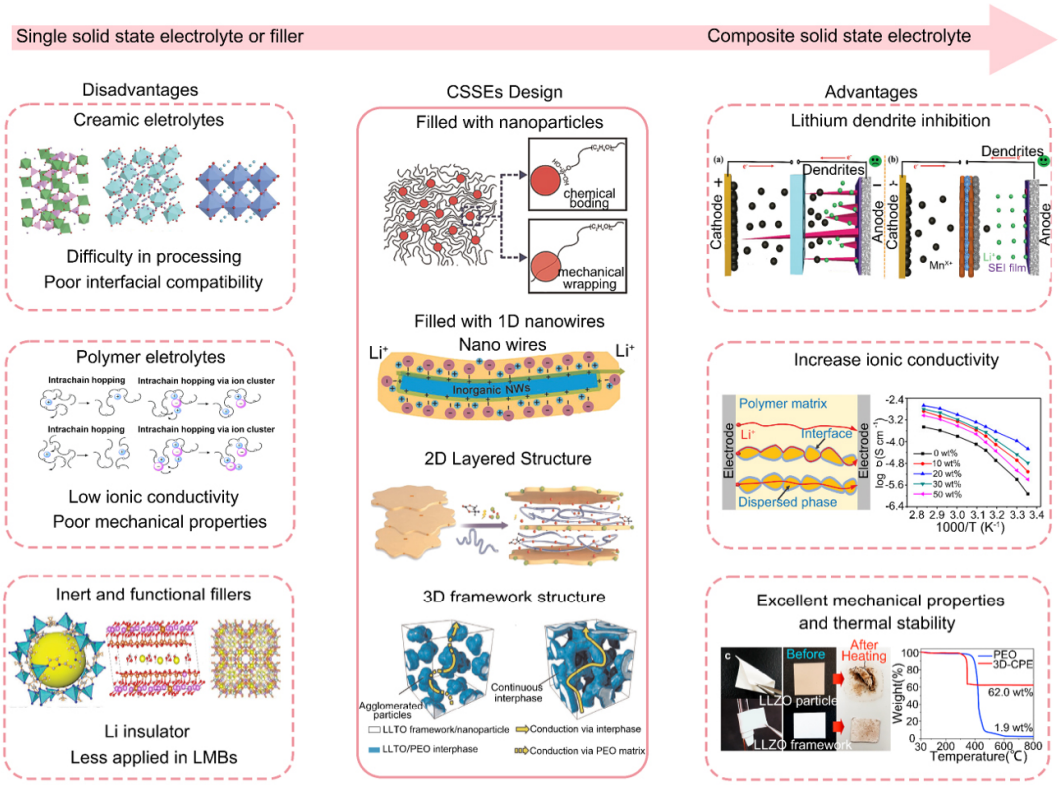

Figure 1. Schematic illustrations of the disadvantages of single SSEs or fillers, advantages of CSSEs, and design methods. Reproduced from Ref.[36] with permission. Copyright 2018, Wiley-VCH. Reproduced from Ref.[27] with permission. Copyright 2023, Wiley-VCH. Reproduced from Ref.[37] with permission. Copyright 2023, Wiley-VCH. Reproduced from Ref.[38] with permission. Copyright 2024, Elsevier. Reproduced from Ref.[39] with permission. Copyright 2021, Wiley-VCH. Reproduced from Ref.[40] with permission. Copyright 2016, American Chemical Society Reproduced from Ref.[41] with permission. Copyright 2016, American Chemical Society Reproduced from Ref.[42] with permission. Copyright 2019, Wiley-VCH. Reproduced from Ref.[43] with permission. Copyright 2018, Wiley-VCH. Reproduced from Ref.[44] with permission. Copyright 2018, Wiley-VCH. Reproduced from Ref.[45] with permission. Copyright 2019, PNAS. Reproduced from Ref.[46] with permission. Copyright 2019, Elsevier.

Lithium-ion channels in CSSEs

By adding fillers to the polymer, more lithium-ion transport channels can be constructed[51], as shown in Figure 2B. Fillers can generally be categorized into lithium-insulated inert fillers and active fillers capable of conducting Li ions, mainly through the following ways to build lithium-ion transmission channels. The inert fillers themselves insulate lithium ions and do not directly facilitate their movement. They function as solid plasticizers inside the polymer matrix, diminishing the polymer's crystallinity. As shown in Figure 2C, incorporating inert fillers into the polymer matrix enhances the amorphous regions of the polymer, hence augmenting lithium-ion transport channels[52]. This behavior can be elucidated by Lewis acid-base theory, in which ether-oxygen bonds in poly(ethylene oxide) (PEO) can provide lone pair electrons. Conversely, numerous inert fillers, including metal oxides, can offer Lewis acid sites to receive lone pair electrons in PEO. The Lewis acid-base interaction facilitated coordination between the filler and the ether-oxygen bond in PEO, hence restricting the arrangement of the PEO chain segments and resulting in reduced crystallinity of PEO. In addition, the Lewis acid-base interaction between the filler and the polymer can provide fast lithium-ion transport channels, as shown in Figure 2D and E; surface treatment of inert fillers with Lewis acid surface groups can facilitate the dissociation of lithium salts, hence enhancing ionic conductivity[53]. The inert filler does not change the transport mechanism of Li ions within the polymer, and the polymer matrix is still capable of transporting Li ions. Therefore, the concentration of the inert fillers should not be

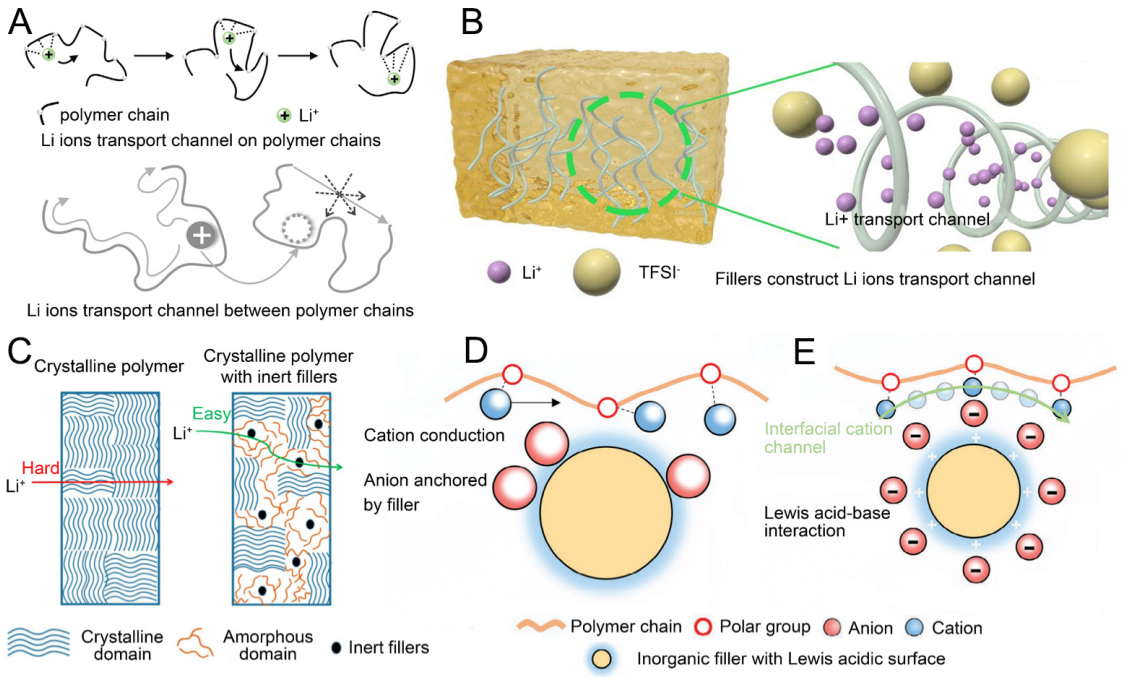

Figure 2. Schematic illustrations of (A) General transport channel of Li ions in polymers[49,50]. Reproduced from Ref.[49] with permission. Copyright 2007, Purpose-LED Publishing. Reproduced from Ref.[50] with permission. Copyright 2023 Wiley-VCH. (B) Fillers construct lithium-ion transport channels[51]. Reproduced from Ref.[51] with permission. Copyright 2023 Wiley-VCH. (C) Inert fillers reduce polymer crystallinity[52]. Reproduced from Ref.[52] with permission. Copyright 2017, Springer Link. (D) Lewis acid-base interaction between filler and polymer enhances cation selectivity. (E) The cation transport pathway is constructed by the Lewis acid-base interaction between filler and polymer[53]. Reproduced from Ref.[53] with permission. Copyright 2024, Wiley-VCH.

too high; otherwise, when the inert filler gathers in the polymer matrix, it will produce a continuous lithium insulation part, which limits the transport of Li ions and reduces the electrochemical properties of the CSSE[54-56].

Unlike inert fillers, active fillers have a unique crystal structure, which makes active fillers Li ions conductors. Lithium-ion transport in active fillers mainly depends on defects in the crystal structure, among which point defects play the most crucial role in ionic transport. According to the point defects, the lithium-ion transport mechanism of active fillers can be classified into two kinds: vacancy and non-vacancy mechanisms. The defect mechanism is further classified into simple vacancy mechanism and vacancy mechanism, and the non-defect mechanism includes an interstitial mechanism and interstitial replacement mechanism[57,58]. Various lithium-ion transport mechanisms are shown in Figure 3A.

The vacancy mechanism involves the diffusion of Li ions from their initial lattice site to an adjacent vacancy. In this process, the atomic jumps produce almost no lattice strain, so the activation energy barrier for the jump is shallow[59]. The lithium-ion transport in the vacancy mechanism depends on the concentration of vacancies in the lattice. In addition, the class of particles in the crystal or the configuration of the doped cations affects the vacancy size to varying degrees, thus influencing the lithium-ion transport in the crystal.

Among the non-vacancy mechanisms, the interstitial mechanism is dominant and divided into direct interstitial diffusion and interstitial knockout diffusion. Direct interstitial diffusion refers to the diffusion of Li ions in the lattice interstitials to the neighboring interstitial sites, which requires the matrix atoms to be

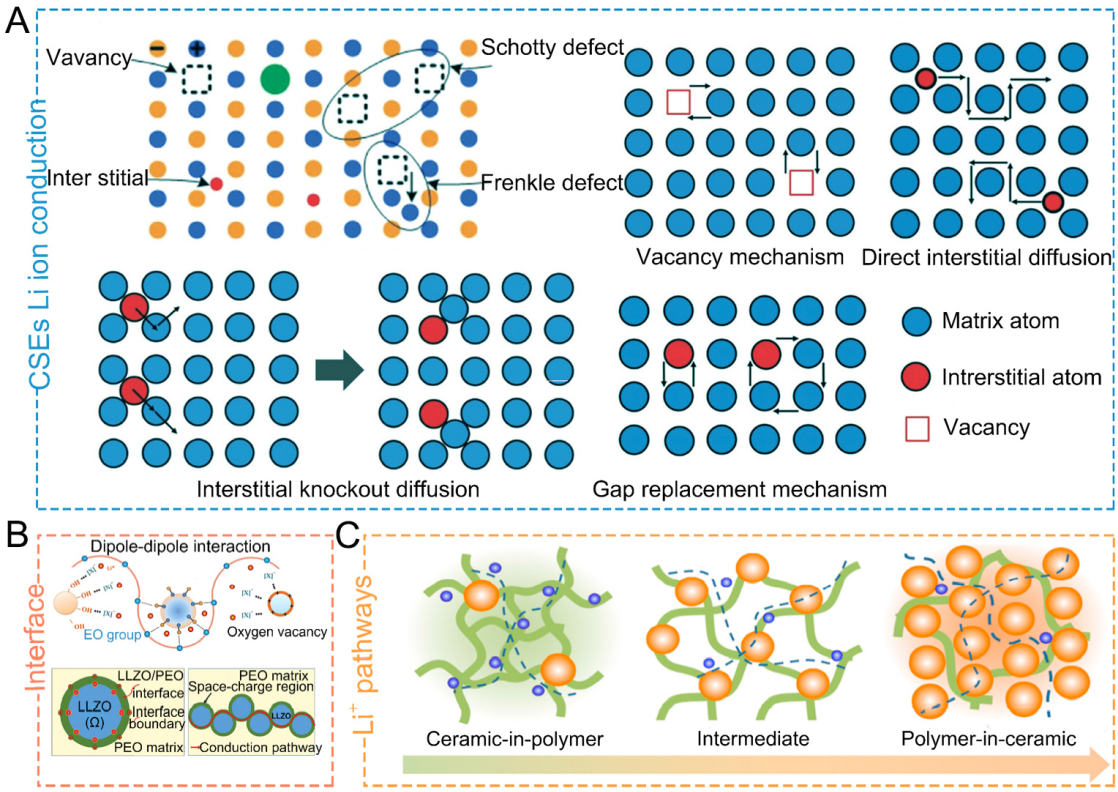

Figure 3. (A) Schematic of Li ions in active fillers[65]. Reproduced from Ref.[65] with permission. Copyright 2020, Royal Society of Chemistry. (B) Interaction of active fillers with polymers and formation of space charge regions[27]. Reproduced from Ref.[27] with permission. Copyright 2023, Wiley-VCH. (C) Lithium-ion transport channels in polymers filled with different concentrations of active fillers[66]. Reproduced from Ref.[66] with permission. Copyright 2017, Elsevier.

much larger than the Li ions in the interstitials, and the migration process creates a considerable lattice strain. In contrast, under the gap knockout diffusion mechanism, the Li atoms in the gap attack the matrix atoms and move into their original positions, while the displaced matrix atoms migrate to nearby gap sites. This mechanism requires that the size of the matrix atoms is not too different from the lithium-ion size and is a standard mode of Li ions diffusion in active fillers. It is divided into direct exchange and ring exchange[60]. The former is a simultaneous movement of two atoms to complete the swap in the lattice position. In comparison, the latter is a ring position exchange by three or more atoms to migrate the atoms to the new lattice position. Compared with the vacancy mechanism, the migration barrier energy of the non-vacancy mechanism is somewhat higher.

When the active fillers are filled into the polymer matrix, Li ions are not transported only in the crystal structure of the active fillers but prefer to be transported at the polymer/active filler interface. As shown in Figure 3B, the incorporation of active fillers induces a chemical reaction between the polymer matrix and the fillers, resulting in space charge zones at the interface of the polymer and fillers[61]. This results in the aggregation of Li ions on one side of the contact. The interconnection of space charge areas generated by each nanoparticle facilitates a continuous and quick transport channel for Li ions, resulting in a substantial enhancement of ionic conductivity. Moreover, as the quantity of active fillers increased, the lithium-ion transport channel was altered accordingly[62]. Figure 3C shows the lithium-ion transport channels in ceramics in polymers, intermediates, and polymers in ceramics, respectively. In the presence of a limited amount of active fillers, the predominant mechanism for the transport of Li ions occurs via the polymer

matrix. When the quantity of active fillers is augmented, there is a tendency for Li ions to be conveyed at the interface between the polymer and active fillers, as well as within the crystals of the active fillers[63-66]. When the active fillers are used as the matrix phase, Li ions tend to be transported mainly in the crystal structure. Even though active fillers can provide more transport channels than inert fillers, the filling concentration still needs to be designed appropriately, and the nanoparticle agglomeration problem still reduces the ionic conductivity of CSSEs.

Key parameters in CSSEs

To better understand the performance of CSSEs, this section focuses on some critical parameters in the performance requirements of CSSEs, including ionic conductivity, lithium-ion transference number, and mechanical properties.

Ionic conductivity

Ionic conductivity (σ) is the paramount characteristic for evaluating lithium-ion transport capability in electrolytes. One of the major problems with SSEs is low ionic conductivity, which allows batteries to operate only at low charge and discharge rates, which is insufficient to run the device[67,68]. The ionic conductivity represents the sum of all mobile charged species (i), which is generally represented by the Arrhenius equation for ion transport in inorganic solid electrolytes (ISEs), as given in[69]

$$\sigma = \sum_i q_i u_i c_i = \sigma_0 \exp\left(\frac{-E_a}{kT}\right) \tag{1}$$

where q_i is the number of charges carried by the charged substance, c_i is the charge concentration, μ_i is the mobility, σ_0 is the pre-factor related to the number of carriers, E_a is the activation energy, k is the Boltzmann constant (1.38×10^{-23} J K^{-1}), and T is the temperature.

In PSEs, ion transport occurs through intra- or inter-chain hopping instead of lattice defect processes. The more dominant view used to describe ion transport in PSEs is the VTF model[67,70], as defined in

$$\sigma = \sigma_0 T^{-\frac{1}{2}} \exp\left(-\frac{B}{T - T_0}\right) \tag{2}$$

where B is the so-called pseudo activation energy in E_a/k and T_0 is the reference temperature, typically 10-50 K below the T_g, this is typically employed to characterize ion transport in PSEs at temperatures exceeding the glass transition temperature of the polymer.

For CSSEs, both equations should be combined if the ionic conductivity is to be calculated. However, attributable to the inclusion of diverse elements such as polymers, lithium salt, and fillers in CSSEs, as well as the various ways of conformity, it is impossible to measure the specific values of the parameters required by the above two equations. Therefore, in practical calculations, one can readily determine the ionic conductivity of CSSEs by employing:

$$\sigma = \sum_i u_i c_i z_i e = \frac{d}{R_b \cdot S} \tag{3}$$

The ionic conductivity of the CSSEs can be calculated using the above equation by positioning SSEs between inert electrodes, such as stainless-steel sheets, and using an electrochemical workstation to determine the impedance (R_b) between the two inert electrodes, with d being the distance between the two working electrodes, generally, the thickness of the SSEs, and S is the area of the working electrode.

In addition to the parameters expressed in Equation (3), the temperature at which the ionic conductivity is measured should also be recorded. CSSEs consist of various ionic conductors, also called Type II conductors, whose ionic conductivity increases with temperature. Consequently, even when the identical electrolyte is assessed at varying temperatures, the ionic conductivity will vary, a feature particularly prevalent in PEO-based CSSEs.

Lithium-ion transference number

Apart from ionic conductivity, the lithium-ion transference number (t_{Li^+}) is an essential indicator of electrolyte performance requirements. The t_{Li^+} represents the percentage of total ionic conductivity accounted for by Li ions in the electrolyte. Electrolytes with elevated t_{Li^+} levels can demonstrate rapid charge and discharge capabilities, even in conditions of poor ionic conductivity[71]. For SSEs (especially PSEs) used in LMBs, the t_{Li^+} can be calculated as a value using the steady state technique, specifically the alternating current/direct current (AC/DC)-based method, combined with DC polarization and impedance spectroscopy. For this purpose, a small DC pulse is applied to a symmetric Li|SSEs|Li symmetric battery. This voltage should not be too high to avoid the decomposition of SSEs, and then the initial (I_0) and steady-state currents (I_{ss}) flowing through the battery, as well as the initial (R_0) and steady-state resistances (R_{ss}) of the two Li interfaces, were measured to calculate the t_{Li^+} according to the Evans-Vincent-Bruce equations as given in[72]

$$t_{Li^+} = \frac{I_{ss}(\Delta V - I_0 R_0)}{I_0(\Delta V - I_{ss} R_{ss})} \tag{4}$$

where ΔV is the DC pulse, and the DC polarization voltage is applied to SSEs. In addition to this, there is another well-established non-electrochemical method to measure the self-diffusion coefficient (D_i) using pulsed magnetic field gradient (PMFG) nuclear magnetic resonance (NMR) and to calculate t_{Li^+} according to[72,73].

$$t_{Li^+} = \frac{D_+}{D_+ + D} \tag{5}$$

where D^+ and D^- are the self-diffusion coefficients for cations and anions, respectively. Anions do not engage in reversible electrochemical reactions; hence, their movement does not convey effective charge.

In traditional PSEs, the lithium-ion transference number is frequently below 0.5 due to the dissociation of lithium salts, resulting in the generation of many anions. In CSSEs, the inclusion of diverse fillers can immobilize anions inside the polymer matrix, hence enhancing the proportion of migrated lithium ions and elevating the lithium-ion transference number beyond 0.5. In addition, if the interface between electrode and electrolyte has a high impedance, Li ions cannot be transferred at the interface. The development of an effective electrode/electrolyte interface is a focal point in the research of CSSEs. The preparation process of CSSEs also has an impact, and the thick electrolyte film will prolong the transport channel of ions and thus

reduce the lithium-ion transference number[74]. Table 1 lists the test parameters for several different types of CSSEs. While these tiny fillers may not constitute a significant proportion of CSSEs, they are essential for improving ionic conductivity, lithium-ion transference number, and other capabilities.

Electrochemical window

The electrochemical window is the primary metric utilized to evaluate the electrochemical stability of CSSEs, denoting the range between the maximum positive and minimum negative potential at which the electrolyte remains stable without undergoing breakdown[96]. In LMBs, the Li^+/Li equilibrium potential of the lithium metal electrode is conventionally established at 0 V. The potential unit of other substances is "V *vs.* Li^+/Li", and most of the current cathode materials are 2~4 V *vs.* Li^+/Li. The highest occupied molecular orbital (HOMO) and lowest unoccupied molecular orbital (LUMO) of the electrolyte determine its electrochemical window, generally requiring the electrolyte to have a lower HOMO than the Fermi energy level of the positive electrode and a higher LUMO than the Fermi energy level of the negative electrode[97,98]. Although CSEs have a wide electrochemical window, they are ineffective in contacting lithium metal, which is one of the problems that CSSEs eliminate. CSSEs can be paired with higher voltage electrode materials due to their wider electrochemical window. This pairing can greatly boost the energy density of LMBs and improve their energy storage capacity. More importantly, a wide electrochemical window can effectively reduce the decomposition of CSSEs during charging and discharging, prolonging the service life of the battery. Consequently, the design of CSSEs with an extensive electrochemical window is crucial for the future advancement of LMBs.

Low interface impedance

The impedance at the interface between the electrode and electrolyte is a crucial factor since excess impedance can result in decreased power density and cycle stability of the battery[99,100]. In contrast to liquid electrolytes that permeate the electrode, stiff SSEs often face challenges in achieving intimate contact with the electrode, leading to inadequate interaction with the lithium anode and elevated charge transfer resistance at the interface. The inclusion of a polymer matrix in CSSEs enhances flexibility, improving adhesion between the electrolyte film and electrode, which facilitates the efficient transport of Li ions from the electrolyte to the electrode and diminishes interface impedance[101,102]. Moreover, by tailoring the electrolyte composition, it is possible to promote the consistent and stable development of the solid-electrolyte interphase (SEI) layer, thereby mitigating side reactions and decreasing the elevated interface impedance resulting from byproducts of these processes[103,104]. However, challenges such as volume expansion/contraction of lithium anode and dendrite growth still contribute to high interface impedance during battery operation[105]. Zhang *et al.* demonstrated effective inhibition of lithium dendrite growth by artificially incorporating 1 wt.% P_2S_5 into the PEO matrix to form Li_2O-rich crystals on the lithium anode surface[106]. Therefore, in designing CSSEs for advanced ASSLMBs, addressing strategies to reduce electrode/electrolyte interface impedance is paramount.

Mechanical properties

Good mechanical properties can ensure that the electrolyte film can maintain the structure integrity under external forces, primarily to inhibit lithium dendrites from penetrating the electrolyte film, mitigate the risk of short circuits or thermal runaway, and guarantee the safety and durability of the battery[107]. Young's modulus of elasticity (E, MPa) and shear modulus (G, MPa) are generally used to evaluate the mechanical strength of CSSEs, as given in[108]

$$E = V_l^2 \rho \frac{(1+\nu)(1-2\nu)}{(1-\nu)} \quad (6)$$

$$G = \frac{E}{2(1+\nu)} \quad (7)$$

Where V_l is the longitudinal velocity, ρ is the density, and ν is Poisson's ratio. Generally, the tensile test can be carried out by the universal material testing machine, and the E and G of CSSEs can be obtained by the stress-strain curve. CSSEs characterized by a shear modulus above 6 MPa have the potential to significantly impede the development of lithium dendrites.

The mechanical strength of CSSEs is significantly affected by the polymer matrix type. For instance, the molecular chain structure of PVDF is more likely to create greater intermolecular forces, whereas the interaction force between the molecular chains of PEO in the linear chain segment is weaker. In comparison to PVDF, the molecular chains of PEO in the linear chain section demonstrate worse mechanical strength. The mechanical strength of CSSEs can be augmented, to a certain degree, by using a ductile filler, as the dispersion of the filler inside the polymer enhances the mechanical properties of CSSEs. The rigidity of inorganic particles can provide better mechanical support. Alongside inorganic fillers, polymers exhibiting high mechanical strength may also be utilized to enhance the flexibility of CSSEs. Du *et al.* incorporated high mechanical strength poly(p-phenylene benzobisoxazole) (PBO) nanofibers into PEO as a supporting skeleton and achieved a tensile strength of 74.4 MPa when the PBO amount was 8 wt.%[109].

Thermal and chemical stability

Excellent thermal stability allows the electrolyte to work stably over a wide range of temperatures, which enables the battery to maintain excellent performance in a variety of extreme environments. Thermal Gravimetric Analysis (TGA) is a technique used to study the mass change of materials during heating and is extremely important for evaluating the thermal stability of CSSEs. When evaluating the thermal stability of CSSEs, place the sample in a TGA instrument, heat it at a programmed temperature, and record the change in its mass simultaneously. By analyzing these data, critical information, such as the temperature at which the electrolyte begins to decompose, the weight loss rate during the decomposition process, and the mass of the final residue can be determined to evaluate the thermal stability of the materials. In general, good CSSEs should be able to maintain a complete structure within the operating range of the battery (generally room temperature to 100 °C) without significant loss of mass. Finally, excellent chemical stability ensures that the electrolyte does not react with the electrode material and degrade. In summary, the comprehensive performance of CSSEs collectively ensures the high efficiency, stability, and safety performance of the battery during use, and is a parameter that should not be ignored when evaluating the performance of CSSEs.

TYPES OF FILLERS IN CSSES

With the introduction of SSEs, PSEs have been gradually studied, but the drawbacks of polymers limit their wide application. The conductivity of polymers mostly relies on the mobility of chain segments within the amorphous area of the polymer. Weston *et al.* first prepared CSSEs in 1982 by filling inert filler α-Al_2O_3 into a PEO/$LiClO_4$ matrix[110]. The inert filler undergoes a Lewis acid-base reaction with the polymer. It functions as a plasticizer, so reducing polymer crystallinity, improving Li-ion mobility, augmenting the amorphous regions of the polymer matrix, and enabling Li ion migration. This CSSE can significantly boost the ionic conductivity to a range of 10^{-5} S cm^{-1} and improve the mechanical strength of electrolytes. The inert fillers under extensive research are primarily categorized as follows: the metal oxide fillers, such as Al_2O_3, SiO_2, and TiO_2; the ferroelectric materials; the carbon materials; the porous materials, such as molecular, metal-organic frameworks (MOFs) materials; and clay materials [111-114].

Table 1. Ionic conductivity and lithium-ion transference number of some CSSEs

Polymer/Lithium salt	Fillers	Size (nm)	Proportion	*T* (°C)	σ (S cm^{-1})	t_{Li^+}	Ref.
PEO/$LiClO_4$	TiO_2	15	10 wt.%	60	2×10^{-4}	0.47	[75]
PEO/$LiCF_3SO_3$	Ti_nO_{2n-1}	2,900	10 wt.%	90	1.8×10^{-4}	0.59	[76]
PVA/PVDF/$LiCF_3SO_3$	SiO_2	84.7	8 mol%	30	1.68×10^{-4}	-	[77]
PEO/LiTFSI	MOF (Uio-66-NH_2/COOH)	-	10 wt.%	60	1.25×10^{-3}	0.36	[78]
PEO/LiDFOB	Al-Li alloy	-	5 wt.%	RT	3.62×10^{-4}	0.52	[79]
PEO/$LiClO_4$	$LiAlO_2$	41	9 mol%	RT	9.76×10^{-5}	-	[80]
PVDF/PVC/LiBOB	ZrO_2	20	2.5 wt.%	20	4.38×10^{-4}	-	[81]
PVDF/LiTFSI	$BaTiO_3$	50	2.5 wt.%	25	1.8×10^{-5}	0.21	[82]
PEO/$LiClO_4$	SBA-15	500	10 wt.%	25	1.9×10^{-5}	0.24	[83]
PEO/LiTFSI	MMT	-	10 wt.%	25	2.75×10^{-5}	0.45	[84]
PVDF/PVA/LiTFSI	OMMT	-	4 wt.%	RT	4.31×10^{-4}	0.4	[85]
PEO/$LiClO_4$	$Li_{0.33}La_{0.56}TiO_3$	50-100	10 wt.%	65	2.8×10^{-3}	-	[86]
PEO/LiTFSI/Pyr_{14}TFSI	$Li_7La_3Zr_2O_{12}$	900	64 wt.%	60	5×10^{-4}	-	[87]
PEGDA/LiTFSI	$Li_{6.4}La_3Zr_{1.4}Ta_{0.6}O_{12}$	50-200	30 wt.%	RT	3.1×10^{-4}	0.43	[88]
PEO/LiTFSI	$Li_{10}SnP_2S_{12}$	-	1 wt.%	50	1.69×10^{-4}	0.38	[89]
PAN/PEO/LiTFSI	$Li_{1.3}Al_{0.3}Ti_{1.7}(PO_4)_3$	-	3D frame	25	6.5×10^{-4}	0.32	[90]
PEO/$LiCF_3SO_3$	$Li_{1.3}Al_{0.3}Sn_{0.35}Ti_{1.35}(PO_4)_3$	-	tablet	RT	4.71×10^{-4}	0.38	[91]
PEO/PPC/LiTFSI	LLTO NWs	500	8 wt.%	60	4.72×10^{-4}	0.23	[92]
PEO/TPU/LiTFSI	LLZO nano-network	250	10 wt.%	60	1.33×10^{-3}	0.37	[93]
PEO/PEG/$LiClO_4$	LATP	-	3D frame	RT	5.2×10^{-5}	-	[94]
PEO/LiTFSI	LLZO	-	3D frame	RT	2.5×10^{-4}	-	[95]
PVA/PEO/$LiClO_4$	LLTO	-	3D frame	25	8.8×10^{-5}	-	[43]

Metal oxide fillers

Among inert fillers, the most widely researched ones are oxide ceramics, such as Al_2O_3, SiO_2, *etc*. Although the mechanical properties of the electrolyte have markedly improved, there is no noticeable improvement in conductivity. The movement of Li ions is mostly influenced by the interface between the inert filler and the polymer. Consequently, the surface modification of the inert filler is essential.

Wang *et al*. used mesoporous SiO_2 with an ultra-high specific surface area and absorbed ethylene carbonate (EC)/propylene carbonate (PC) plasticizer in its nanopores to make SiO_2 as ionic active fillers[115]. The electrolyte film was prepared by adding the above fillers to PEO/$LiClO_4$ at a ratio of 10 wt.%, and the ionic conductivity of the electrolyte could be enhanced to 1.5×10^{-4} S cm^{-1}. The observed phenomenon can be attributed to the Lewis acid-base interactions between the specific surface state of active SiO_2 and the polymer chains, as well as the anions of lithium salts. Additionally, the presence of the EC/PC plasticizer in the nanopores acts synergistically to enhance the dissociation of the $LiClO_4$ and facilitate the rapid ionization of the Li ions, thereby promoting efficient lithium-ion transport. Wang *et al*. designed SiO_2 with a hydroxyl-rich surface, which was prepared *in situ* using hydrolysis of tetraethyl orthosilicate (TEOS) in an alkaline solution and dispersed in PEO/LiTFSI/succinonitrile (SN)[116]. The prepared electrolyte connects PEO and SN by forming hydrogen bonds between the hydroxyl groups on the surface of SiO_2 and C, N, and F atoms. On the one hand, the addition of SiO_2 nanoparticles reduces the crystallinity of PEO, while on the other hand, it enhances the mechanical strength and the ionic conductivity of the electrolytes. Tang *et al*. utilized poly(propylene oxide)-poly(ethylene oxide)-poly(propylene oxide) triblock main chains and surface-modified SiO_2 nanoparticles to create a unique cross-linked nanocomposite polymer electrolyte

(CNPE)[117]. Incorporating 10 wt.% SiO_2 resulted in a room temperature conductivity of 1.32×10^{-3} S cm^{-1} and excellent mechanical stability (elongation of 700%). The enhancement is ascribed to the diminished crystallinity of PEO resulting from the incorporation of SiO_2 and the augmented hydrogen bonding facilitated by ethyl carbamate groups in CNPE, leading to improved particle conductivity and mechanical properties. Furthermore, filler surface treatment improves compatibility with the polymer matrix, creating additional migration paths for Li ions while reducing polymer matrix crystallinity and enhancing adhesion for superior mechanical properties in CSSEs.

While the incorporation of fillers can improve the characteristics of the polymer matrix, there is a critical limit for the amount of fillers utilized. It has been shown that when the inert filler content is below the threshold, lithium-ion transport is facilitated through interaction with the polymer and lithium salt. However, when the content is higher than the critical value, the fillers are subject to agglomeration problems. The agglomeration problem diminishes the effect of inert fillers on reducing polymer crystallization, and Li ions are blocked at the agglomerates as they are transported through the electrolyte[118]. More seriously, the aggregation of inert filler particles at the anode interface leads to rapid deposition of lithium dendrites, significantly reducing the life of electrolytes. Therefore, it is crucial to reduce the concentration of the filler to obtain a homogeneous distribution inside the polymer matrix. Multiple scholarly investigations have proposed possible remedies to tackle the problem of agglomeration.

Zhan *et al.* prepared porous SiO_2 particles (10 wt.%) with vinyl groups, which were interconnected with the cross-linking agent polyethylene glycol diacrylate (PEGDA) to achieve an interconnected network structure in the PEO matrix, which could achieve a uniform distribution of fillers[119]. As shown in Figure 4A and B, the uniformly distributed filler can better inhibit the crystalline behavior of PEO. It can establish chemical linkages inside the polymer matrix, therefore enhancing the compatibility at the interface between the polymer and the inorganic filler. Bao *et al.* deposited ZnO quantum dots into the PEO matrix using the vapor-phase infiltration (VPI) method, which can achieve the average dispersion of ZnO quantum dots in PEO, As shown in Figure 4C[120]. The crystalline behavior of PEO is inhibited by the strong interaction of ZnO with the PEO polymer chains. In addition, certain ZnO quantum dots persist on the electrolyte surface, creating a Li-Zn alloy with the lithium anode, therefore markedly decreasing the interfacial resistance.

It is not difficult to see that the role of metal oxide fillers in CSSEs is very limited, and most of them need to be pre-treated or rely on advanced preparation technology to achieve the improvement of CSSE performance. Therefore, there is relatively little research on inert fillers, and materials with special functions can provide more performance improvements for CSSEs.

Ferroelectric materials fillers

In addition to the studies of some joint oxide fillers mentioned above, many scholars apply ferroelectric materials to electrolytes[121]. Although ferroelectric materials are mainly applied as catalysts in electrocatalysis in previous studies, some scholars have found that, in addition to lowering the crystallinity of polymers, Ferroelectric materials can impede the proliferation of lithium dendrites through their spontaneous polarization phenomena[122]. Taking the most traditional $BaTiO_3$ (BTO) as an example, Ti^{4+} with a small radius is located in the center of an octahedron consisting of six O^{2-}, while O^{2-} is squeezed in the middle of Ba^{2+} with a larger radius. When the BTO is filled into the electrolyte, the electrostatic field inside the battery causes the centers of the O^{2-} and Ti^{4+} in the batteries of the BTO to no longer coincide, which causes a spontaneous polarization from negative to positive charge[121]. This polarization phenomenon draws Li ions from the electrolyte, facilitating accelerated transit of Li ions within the electrolyte and

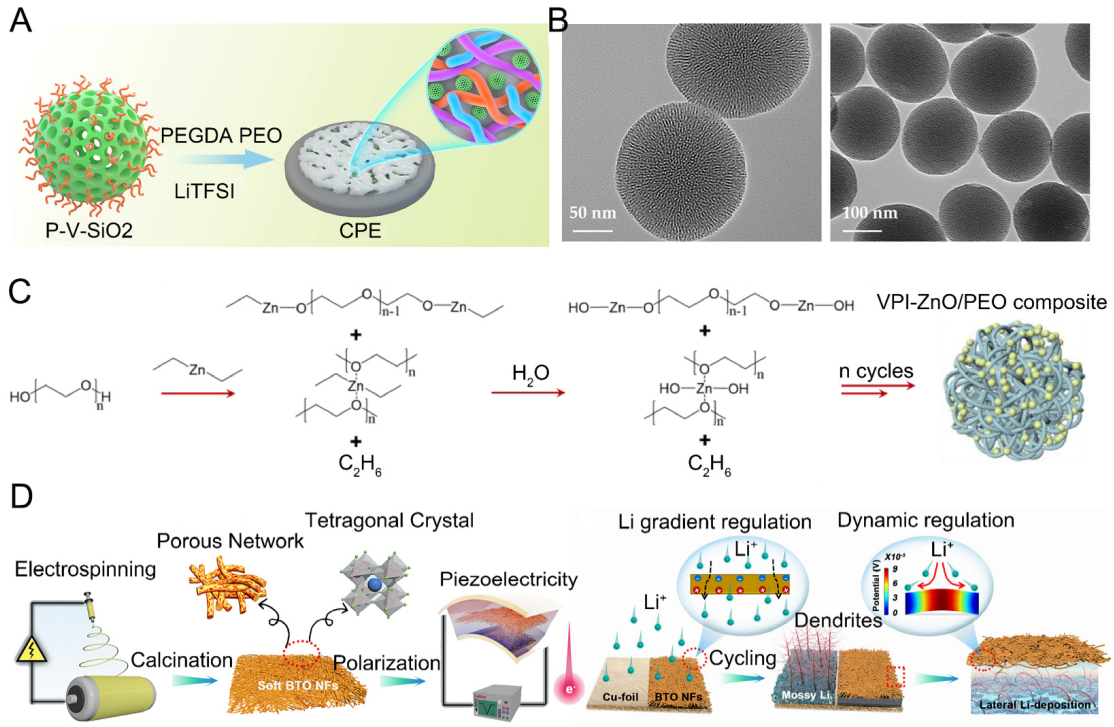

Figure 4. (A)Schematic illustration of uniform dispersion of p-V-SiO_2 in PEO. (B) SEM image of p-V-SiO_2[119]. Reproduced from Ref.[119] with permission. Copyright 2021, Licensee MDPI. (C) Schematic illustration of the VPI process[120]. Reproduced from Ref.[120] with permission. Copyright 2021, Elsevier. (D) BTO NF films modulate lithium dendrite growth at copper electrodes[121]. Reproduced from Ref.[121] with permission. Copyright 2021, American Chemical Society.

diminishing the concentration gradient of Li ions at the anode. In addition, the growth of lithium dendrites on the anode causes the BTO in the electrolyte to deform by accumulating stresses at the lithium dendrites. A study connecting BTO ceramic nanofibers (BTO NFs) with Cu collectors to detect the growth of lithium dendrites, as shown in Figure 4D. Positive induced charges are generated on the upper side of the deformation position to inhibit the growth of lithium dendrites at the center of deformation. In contrast, negatively generated charges on the bottom side attract lithium ions, enabling their transit perpendicular to the development direction of lithium dendrites, hence promoting uniform lithium deposition.

Singh and Chandra[123] reported $Ba_{0.7}Sr_{0.3}TiO_3$ and $Ba_{0.88}Sr_{0.12}TiO_3$ materials; these materials significantly enhance the electrolyte conductivity by a factor of ten when 3 wt.% of them are included into PEO. Affected by the distribution of the local electric field inside the polymer matrix, the dielectric constant of the ferroelectric material affects the ion transport mode in the polymer electrolyte. The elevated dielectric constant of the ferroelectric material, in contrast to the polymer matrix, leads to an intensified electric field at the interface between the polymer and the ferroelectric material. Firstly, this phenomenon results in the facilitation of ion movement towards the interface between the polymer and filler. Secondly, as the lithium salt approaches the polymer-filler interface, its dissociation becomes more pronounced, leading to a higher concentration of Li ions in the electrolyte and thereby improving the ionic conductivity.

Carbon materials fillers

In previous studies, carbon nanotubes (CNTs) have generally been used as anode materials, and several investigations have been undertaken to include them into polymer electrolyte matrices owing to their superior mechanical strength and elevated aspect ratio[124,125]. Li ions can be transported rapidly along the

CNT/substrate interface, and the elevated electron cloud density of CNTs can significantly interact with Li ions, facilitating the dissociation of lithium salts. However, the electronic conductivity of CNTs is prone to short-circuiting in batteries, which limits their application as polymer electrolyte fillers[126].

Tang *et al.* grew one-dimensional CNTs in the middle of two layers of montmorillonite (MMT) flake crystals, as shown in Figure 5A[127]. The growth of CNTs within the sandwich resulted in the exfoliation of the MMT flake crystals to form a composite material with a high aspect ratio. The use of PEO markedly improves the mechanical characteristics of the polymer matrix and enhances ionic conductivity, and the highest ionic conductivity of 2.07×10^{-5} S cm^{-1} was reached at a filler dosage of 10 wt.%. Meanwhile, the electron transport on the CNTs is blocked by the MMT attached, hence decreasing the chance of short-circuiting in the battery. Wang *et al.* used a solution casting method to cast the CNTs or fullerenes (C_{60}) filled into hyperbranched star polymer HBPS-(PMMA-b-PPEGMA)$_{30}$ to prepare CSSEs. The addition of carbon material only decreases the T_g of the polymer matrix slightly[128]. However, the decomposition temperature of both CSSEs prepared can reach 383 °C due to the high thermal stability of the carbon material itself. The ionic conductivity of the 0.2 wt.% CNT-filled electrolyte attains 1.06×10^{-5} S cm^{-1}, while the lithium-ion transference number is 0.52, which shows high chemical stability above 5.2 V. In contrast, all the performances of the C_{60}-filled electrolyte are poorer. There are few studies on carbon materials as fillers, and there are still many questions about the detailed mechanism of ionic conductivity enhancement of CSSEs, which need further research.

The research on carbon materials as fillers for CSSEs is relatively limited, primarily due to the electronic conductivity of carbon materials. The advancement of interface design engineering to address the conduction issue in CSSEs filled with carbon materials at the electrode interface is anticipated to drive further progress in this area.

Clay materials fillers

MMT is a more widely studied material because of its high specific surface area and cation exchange capacity. It is a silica-aluminate with a unique layered structure, with one Al-O octahedra layer sandwiched between two Si-O tetrahedra layers and with suspended hydrated cations in the MMT layer. Li ions can easily replace these cations, and the migration energy barrier of Li ions is as low as 0.16 eV. The -OH groups are also present at the edges of the MMT to form Lewis acid sites, which can anchor the TFSI$^-$s and thus facilitate the transport of Li ions. Zhu *et al.* cured the PVC-s-MMT, which is rich in hydroxyl groups on the surface, with poly(vinyl carbonate) (PVC) by a cross-linking agent so that it can be dispersed uniformly and have good interfacial compatibility[129]. The conductive mechanism of PVC-s-MMT is illustrated by density functional theory (DFT) calculations. As shown in Figure 5B, the coupling technique enhances interfacial channels for lithium ions, diminishes their interaction with the oxygen atom in the carbonyl group, and reduces the migration barrier for Li ions. The ionic conductivity is 7.9×10^{-5} S cm^{-1} when the dosage of MMT is 2 wt.%. As shown in Figure 5C, the Li|PVC-s-MMT|Li battery has a very low overpotential. Meanwhile, as shown in Figure 5D and E, the battery consisting of a Li anode and an LFP cathode exhibits good multiplicative performance and reversibility with a smooth platform. Zhao *et al.* prepared LOPPM electrolyte films by adding 20 wt.% organically modified MMT (OMMT), which is rich in Lewis acid centers, to poly(methyl methacrylate) (PMMA)/PVDF/P[VDF-hexafluoropropylene (HFP)], which possessed ionic conductivity of 1.1×10^{-3} S cm^{-1} and lithium-ion transference number of 0.54 at room temperature[130]. This was attributed to the interaction of MMT with PVDF, which uniformly dispersed in PMMA and constructed unique multi-facial channels. As shown in Figure 5F, the negative charge on the surface of OMMT adsorbs Li ions and thus facilitates the transport of Li ions. Moreover, LOPPM exhibits excellent stability and compatibility with lithium anode; the assembled Li|LOPPM|Li symmetric battery can be cycled continuously for 200 h.

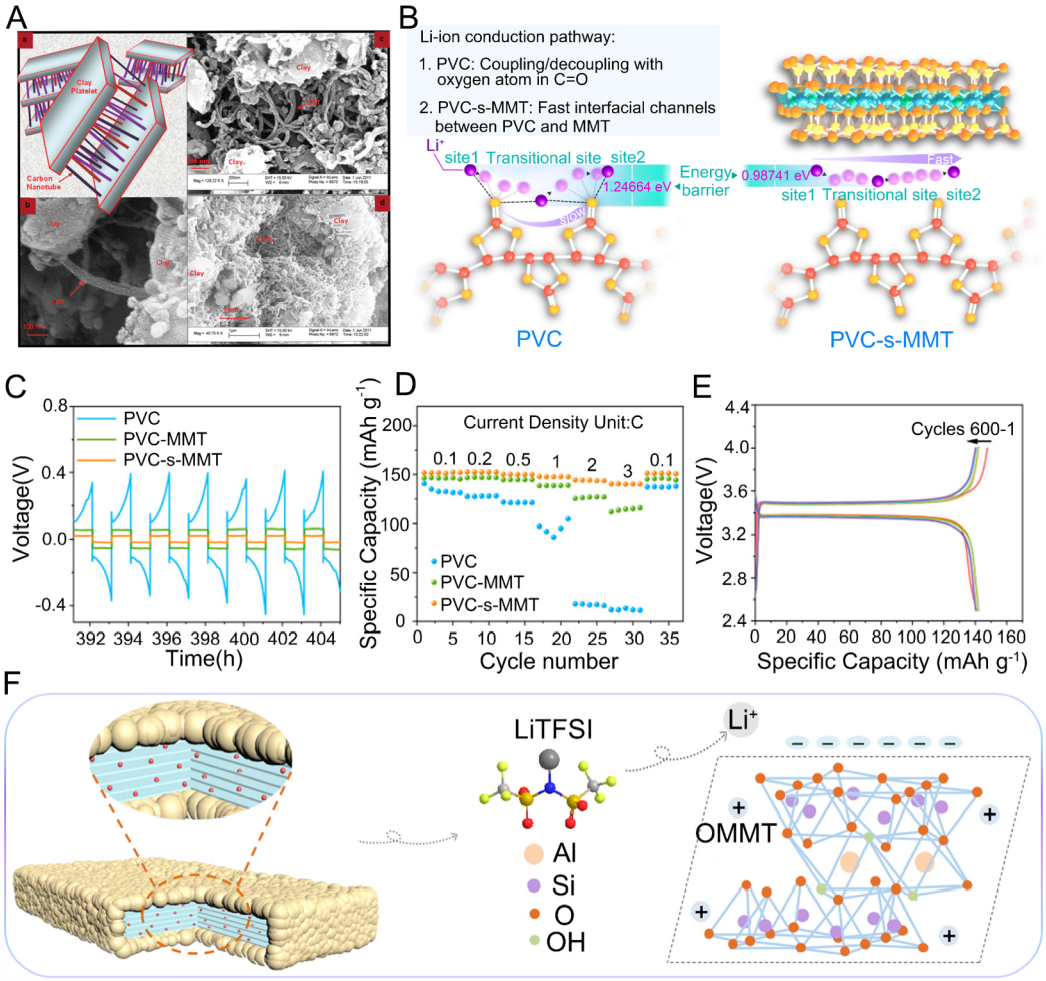

Figure 5. (A) Schematics of montmorillonite clay-CNT hybrid fillers and SEM images of clay-CNT structures at various magnifications[127]. Reproduced from Ref.[127] with permission. Copyright 2012, American Chemical Society. (B) Migrating behavior of Li ions on PVC-s-MMT interphase and PVC electrolyte. (C) Galvanostatic cycling curves of lithium symmetrical battery utilizing the PVC, PVC-MMT, and PVC-s-MMT at the current density of 0.1 mA cm^{-2}. (D) Rate capacity of PVC-s-MMT at different current densities. (E) Discharge/charge profiles for Li|PVC-s-MMT|LFP battery at 1 C at room temperature[129]. Reproduced from Ref.[129] with permission. Copyright 2024, American Chemical Society. (F) Schematic illustration of OMMT promoting lithium-ion migration[130]. Reproduced from Ref.[130] with permission. Copyright 2023, Wiley-VCH.

Porous materials fillers

MOFs enhance electrolyte performance by leveraging their elevated specific surface area and additional characteristics[131,132]. The elevated porosity and specific surface area of MOF materials dictate their high surface energy, which can adsorb some side reaction products and impurities. Moreover, MOF materials have diverse structures that can be adapted to various materials so that these materials can be easily compounded with other materials.

Due to its high surface polarity, the electrochemical performance can be enhanced by modulating the Lewis acid-base interaction in the electrolyte system. Lu *et al.* designed a bifunctional N-CP@Sn-MOF material, an excellent precursor of lithium-philic accelerators, which can be used as a good filler in polymers[133]. By utilizing nitrogen atoms in the host material as nucleation sites for lithium, the overpotential of lithium nucleation can be reduced, facilitating the consistent deposition and stripping of lithium metal on the host material during the charging-discharge cycle. Filling it into the PEO matrix increased the lithium-ion

transference number from 0.194 to 0.367, and the electrochemical window from 3.8 to 4.5 V. Wang *et al.* utilized the adsorption capacity of the typical MOF HKUST-1 (Cu) to accommodate Li ion liquid (Li-IL) in the pores to form ion-conducting Li-IL@HKUST-1[134]. The Li-IL@HKUST-1 additive, which exhibits ionic conductivity, can efficiently enhance the polymer matrix by a novel ionic conductive network. This leads to an improvement in ionic conductivity and guarantees the even distribution of lithium. The CSSE was prepared by solution casting after mixing Li-IL@HKUST-1 with PEO, and the ionic conductivity was 1.2×10^{-4} S cm^{-1} at 30 °C.

A molecular sieve is a substance characterized by homogeneous micropores, extensively utilized across various domains, and serves as a typical low-cost, environmentally sustainable filler[135]. Molecular sieve materials have more robust Lewis acid centers in their backbones and channels, making them more effective in reducing polymer crystallization. Jiang *et al.* filled SBA-15 molecular sieve material into PVDF-HFP, which has stable electrochemical properties because the backbone unit of SBA-15 consists of SiO_2 and has a larger pore size, making the structure more stable[136]. The prepared CSSE has an ionic conductivity of 5×10^{-5} S cm^{-1} at room temperature, and SBA-15 can also absorb a small number of impurities in the electrolyte, reducing the effect of impurities on the Li anode. Zeolite is a typical microporous material among molecular sieves with extremely high specific surface area. Chang *et al.* used commercially available zeolite to condition a typical carbonate-based electrolysis [1 mol L^{-1} $LiPF_6$-EC/dimethyl carbonate (DMC)] without adding any additional salt or additives[39]. The prepared electrolyte could exhibit enhanced antioxidant stability at 4.6 V and 55 °C. Long cycle life and ultra-stable Li|CSSE|NCM-811 batteries were successfully obtained with 83.2% capacity retention after more than 1,000 electrochemical cycles. Ding *et al.* developed an electrolyte utilizing physicochemical X-type zeolite (Li-X), incorporating 3 wt.% Li-X into PVDF-HFP[137]. The resultant electrolyte layer demonstrated a notable ionic conductivity of 1.98×10^{-4} S cm^{-1}, a substantial lithium-ion transference number of 0.55, and an extensive electrochemical window of 4.7 V. Zeolites featuring Lewis acid sites enhance the availability of free Li ions and serve to anchor the N,N-dimethylformamide (DMF) and PVDF-HFP polymer chains, thereby reducing polymer crystallinity and safeguarding the lithium metal anode.

These novel materials facilitate enhanced interaction between fillers and polymers, thereby improving the application performance of CSSEs in terms of mechanical properties, electrochemical windows, and electrode/electrolyte interface. This improvement is achieved not only through the reduction of polymer crystallinity to enhance ionic conductivity but also by providing a greater development potential than traditional metal oxide fillers.

Unlike inert fillers, active fillers contain Li ions and rely on the movement of vacancies or interstitial ions to rapidly transport Li ions. Therefore, active fillers are believed to be more efficacious in enhancing the electrochemical performance of CSSEs. The types of active fillers studied include perovskite, garnet, NASICON, and so on.

Perovskite and anti-perovskite type fillers

The general chemical formula of perovskite is ABO_3, as shown in Figure 6A, where A and B are the cations' six and twelve oxygen coordination sites, respectively. The A site is the octahedral void, typically inhabited by cations with greater ionic radii, such as Na^+, K^+, Ca^{2+}, Ba^{2+}, La^{3+}, *etc.* The B site is the center of the octahedron, which is occupied by cations with smaller ionic radii and forms an octahedral coordination site with the six oxygen ions, such as Sc^{3+}, Al^{3+}, Ti^{4+}, Ge^{4+}, Nb^{5+}, and so on[138]. The most studied perovskite fillers are namely $Li_{3x}La_{2/3-x}TiO_3$. Generally speaking, LLTO is a cubic crystal system, and a large number of TiO_6 octahedra connected by co-topography form the basic skeleton of LLTO crystals, and Li ions and La^{3+} can

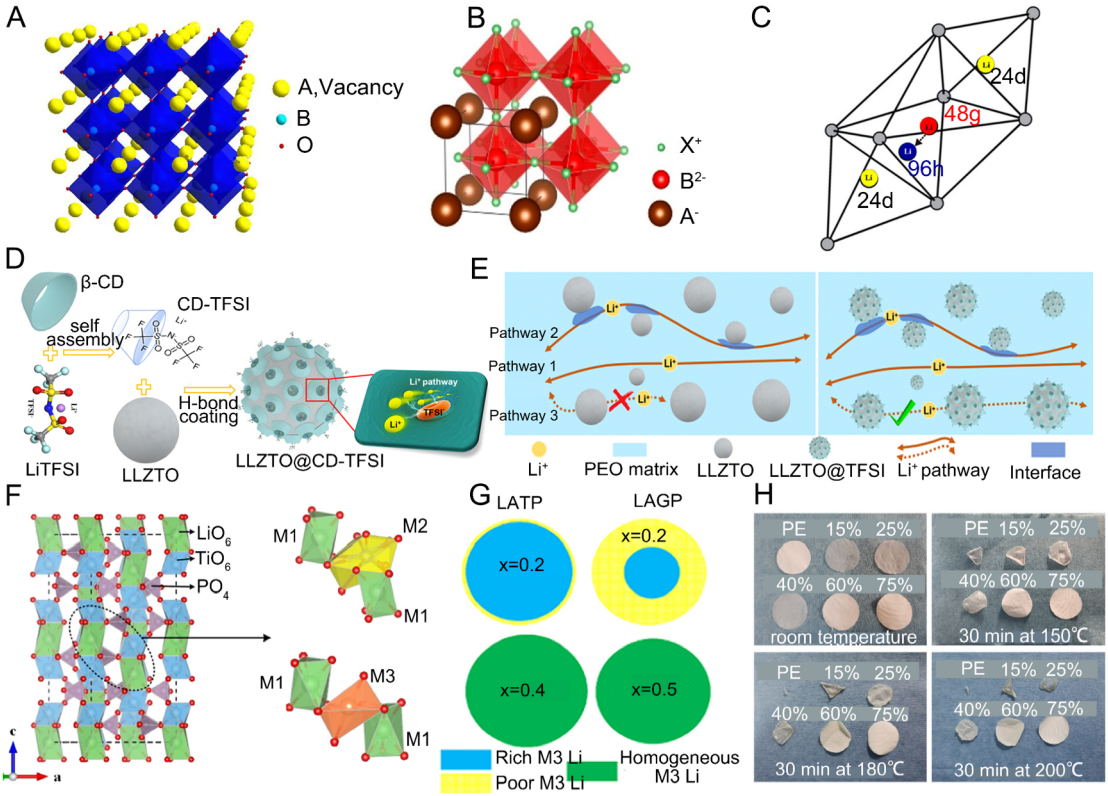

Figure 6. (A) Crystal structure of cubic perovskite[138]. Reproduced from Ref.[138] with permission. Copyright 2021, Springer Link. (B) Octahedral framework model of cubic X_3BA anti-perovskite[153]. Reproduced from Ref.[153] with permission. Copyright 2022, American Chemical Society. (C) Distribution of Li ions in tetrahedral (24d) and octahedral positions (48g and 96h)[157]. Reproduced from Ref.[157] with permission. Copyright 2020, American Chemical Society (D) Schematic illustration of the process for preparing CD-TFSI supramolecular combination modified LLZTO. (E) Schematic illustration of lithium-ion channel in PEO/LLZTO@CD-TFSI[176]. Reproduced from Ref.[176] with permission. Copyright 2022, Wiley-VCH. (F) Crystal structure of $LiTi_2(PO_4)_3$ and M1, M2, and M3 sites of Li ions[179]. Reproduced from Ref.[179] with permission. Copyright 2021, Wiley-VCH. (G) Distribution of Al/Li phases in LATP and LAGP with varying Al concentrations. Yellow regions signify deficient Al/Li phases, while blue regions denote abundant Al/Li particles. Green areas represent uniform materials[181]. Reproduced from Ref.[181] with permission. Copyright 2014, Elsevier. (H) Variation of the CSSE films with different LAGP contents and PE skeleton at different temperatures and holding times[196]. Reproduced from Ref.[196] with permission. Copyright 2022, Elsevier.

be homogeneous in the interstices of these octahedra[139,140]. However, LLTO will also have tetragonal phases, leading to the uneven distribution of La^{3+}. The ion vacancy mechanism predominantly governs the migration of Li ions in LLTO. The vacancy of La sites is necessary for lithium-ion conductivity, and the dimensions of the anionic A and the vacancy concentration will influence the ionic conductivity of perovskite electrolytes. The LLTO-type electrolyte is stable and relatively simple to prepare, and its ionic conductivity can reach up to 10^{-3} S cm^{-1}. Nevertheless, the assessed ionic conductivity frequently falls below 10^{-4} S cm^{-1}. Table 2 shows the crystal synthesis method and properties of some perovskites and anti-perovskites.

LLTO electrolytes were used directly as an SSE layer to match electrodes and make solid-state batteries. However, the rigid electrolyte/electrode interface creates a tremendous interfacial impedance that limits this application. In addition, a significant problem with LLTO is that when LLTO is in contact with lithium metal, lithium can easily and rapidly insert into the LLTO structure, reducing Ti^{4+} to Ti^{3+}, increasing the electronic conductivity, and causing an internal short circuit[151]. Therefore, subsequent studies started to compound LLTO with PSEs, effectively solving the problem of poor interfacial contact while preventing

Table 2. The crystal synthesis method and properties of some perovskites and anti-perovskites

Composition	Synthesis method	Sintering temperature (°C)	σ (S cm^{-1}) /T (°C)	Ref.
$Li_{0.25}La_{0.583}TiO_3$	Solid-state reaction	1,000	4.53×10^{-4}/20	[141]
$Li_{0.33}La_{0.557}TiO_3$	Sol-gel processing	1,000	3.9×10^{-3}/RT	[142]
$Li_{15/56}Sr_{1/16}La_{15/28}TiO_3$	Solid-state reaction	1,100	4.84×10^{-4}/25	[143]
$Li_{0.225}La_{0.625}Al_{0.1}Ti_{0.9}O_3$	Solid-state reaction	1,000	3.23×10^{-4}/20	[141]
$Li_{0.355}La_{0.35}Sr_{0.3}TiO_3$	Solid-state reaction	1,300	2.78×10^{-5}/RT	[144]
$Li_{0.33}La_{0.46}Y_{0.1}TiO_3$	Sol-gel processing	1,350	9.51×10^{-4}/25	[145]
Li_2OHCl	Solid-state reaction	300	1.9×10^{-3}/100	[146]
$(Li_2OH)_{0.99}K_{0.01}Cl$	Solid-state reaction	400	4.5×10^{-3}/25	[147]
Li_2OHBr	Solid-state reaction	200	1.6×10^{-6}/25	[148]
Li_3OCl	Pulsed laser deposition	300	2×10^{-4}/RT	[149]
$Li_{2.99}Ba_{0.005}OCl$	Hydrothermal reaction	250	7.65×10^{-3}/RT	[150]

direct contact between LLTO and Li. Romero *et al.* added LLTO of different sizes to PMMA, and an order of magnitude enhanced the ionic conductivity of the CSSE compared to the pure PMMA electrolyte[152]. The CSSE had the highest room temperature ionic conductivity (1.13×10^{-4} S cm^{-1}) when the average grain size of LLTO was 50 nm. In addition to LLTO, $Li_{3/8}Sr_{7/16}Ta_{3/4}Zr_{1/4}O_3$ (LSTZ) has attracted many studies due to its excellent stability in humid environments. Research indicates that nearly no insulating phase develops on the surface of LSTZ, leading to minimal interfacial resistance between LSTZ and PEO. Xu *et al.* prepared a PEO/LiTFSI/LSTZ electrolyte using LSTZ as fillers, which had ionic conductivity of 5.4×10^{-5} S cm^{-1} at 25 °C[45]. Perovskite-type electrolytes can efficiently impede the crystallization of polymer electrolytes while offering strong ionic conductivity, but to obtain perovskite electrolyte materials with stable crystal structures, high sintering temperatures or the addition of various sintering aids are often required. Therefore, the cost of perovskite materials is generally high, and there remains a large gap between the performance of perovskite electrolytes prepared by low-temperature sintering and those prepared under high-temperature conditions.

Anti-perovskite has the same crystal structure and stoichiometric ratios as perovskite, with the general chemical formula X_3BA. However, unlike perovskite, as shown in Figure 6B, the anion (B) in anti-perovskite occupies the center of the octahedron. At the same time, the cation (X) is located at the apex of the octahedron[153,154]. X is a monovalent cation, generally an alkali metal; B is a divalent anion, such as O^{2-} and S^{2-}, and A is a monovalent anion, generally for the halogen elements[155]. Unlike perovskite electrolytes, the concentration of Li ions is higher in anti-perovskite. Li ions in perovskite structures are generally located in the A or B sites, with a maximum lithium-ion concentration of only 20 at%, primarily due to the necessity for cations with greater radii to occupy the A sites, hence ensuring the stability of the crystal structure. In contrast, the lithium-ion concentration in the X-site of perovskite can reach 60 at%, which has the potential to dramatically increase the ionic conductivity of the electrolyte and solve the problems caused by the reduction of high-valent metals in conventional perovskite electrolytes.

Ye *et al.* prepared CSSE by incorporating lithium-rich anti-perovskite Li_2OHBr as a filler into PEO[156]. At 5 wt.% Li_2OHBr dosage; the electrolytes had a conductivity of up to 4.5×10^{-4} S cm^{-1} (60 °C). The electrolyte containing Li_2OHBr improves the cycling stability and multiplication performance in batteries with a 3D-structured lithium/copper mesh composite anode and LFP cathode. The easy processing, low cost, and environmental friendliness of the anti-perovskite electrolyte make it more readily available for application, and it has exceptional stability when in contact with the lithium metal. However, the electrochemical

window of perovskite electrolytes is narrow, and they generally decompose around 3 V, which makes them less stable for most of the commonly used cathode materials.

While perovskite electrolytes offer broad options and demonstrate excellent performance, their preparation often necessitates harsh conditions. For instance, producing cubic crystalline LLTO electrolytes requires very high sintering temperatures or the addition of various sintering additives and new synthesis technologies. Additionally, the preparation process for anti-perovskite often calls for an inert atmosphere. Consequently, achieving large-scale application of CSSEs based on perovskite-type fillers presents a significant cost challenge.

Garnet type fillers

The general chemical formula of a typical garnet type is $A_3B_3C_2O_{12}$, with A = Ca, Mg, Y, La or rare-earth metals, B = Bi, Ge, Al, and C = Al, Fe, Ga, Ge, Mn, Ni, or V. Its A, B, and C are 8, 4, and 6 oxygen-coordinated cationic sites, respectively, which crystallize in a face-centered cubic structure. As shown in Figure 6C, Li ions occupy various vacancies within the garnet structure, namely tetrahedral vacancies (24d), octahedral vacancies (48g), and eccentric octahedral vacancies (96h)[157-159]. The above tetrahedra and octahedra share faces to form a 3D network structure, allowing fast lithium-ion transport. The enhancement of ionic conductivity due to the incorporation of garnet electrolytes into the polymer matrix is closely associated with the space charge region. The presence of space charge regions enables the migration of Li ions from garnet lattice sites to surface sites, especially in the presence of negatively charged vacancies inside the lattice and positively charged Li ions at the surface[160,161]. When the space charge layer regions near each nanoparticle are interconnected, a channel available for rapid lithium-ion transport is constructed. The garnet-based electrolyte that has been studied more is the LLZO-type electrolyte. Murugan *et al.* first proposed LLZO-type electrolytes in 2007, which can reach a room-temperature ionic conductivity of 3×10^{-4} S cm^{-1}, which attracted the attention of many scholars, resulting in many studies on the modification of the LLZO-based electrolyte[162]. Table 3 shows the crystal synthesis method and properties of some Garnets. Chen *et al.* used a casting method to prepare the CSSE film from PEO and 7.5 wt.% LLZO[173]. The compliant electrolyte film had the maximum ionic conductivity (5.5×10^{-4} S cm^{-1}) at 30 °C due to the synergistic effect of cubic LLZO.

LLZO structures can form both cubic and tetragonal phases, and many studies have shown that cubic-structured LLZOs have higher ionic conductivity. To obtain stable cubic-structured LLZO, the three cationic sites of LLZO are usually doped and modified using cations. Karthik *et al.* synthesized Al-doped $Li_{6.28}Al_{0.24}La_3Zr_2O_{12}$ (Al-LLZO) electrolyte using the solid-state reaction method, which was added to the PEO/$LiClO_4$ matrix to prepare a CSSE film[174]. When the amount of Al-LLZO was 20 wt.%, the CSSE had an ionic conductivity of 4.4×10^{-4} S cm^{-1} at 30 °C. Nguyen *et al.* prepared co-doped LLZO (NAL) with Al^{3+} and Nb^{5+} using the sol-gel method, and X-ray diffraction (XRD) proved that NAL had a stable cubic phase[175]. The PEO-NAL-LiTFSI-SN electrolyte film prepared with PEO as the substrate possessed an ionic conductivity of 3.09×10^{-4} S cm^{-1} at room temperature, and NAL not only facilitated the lithium-ion transport channel but also immobilized anions to enhance the solubility and transport of more Li ions. In addition, there have been more studies on Ta-doped $Li_{6.75}La_3Zr_{1.75}Ta_{0.25}O_{12}$ (LLZTO) electrolytes, and the CSSE system of LLZTO with PEO is considered to have a promising future. However, the surface wettability of PEO and LLZTO is poor, and the interfacial problem between the two has always existed. The interface between PEO and LLZTO can be efficiently modified to enhance their physical and electrochemical properties. Lu *et al.* designed β-cyclodextrin (CD) supramolecules containing self-assembled LiTFSI salts to modify the interface of LLZTO[176]. The preparation process is shown in Figure 6D, where LiTFSI self-assembles within the cavity of β-CD through host-guest interactions, while β-CD associates with LLZTO via hydrogen bonding. The electrolyte film of PEO/LLZTO@CD-TFSI prepared by compositing with PEO had

Table 3. The crystal synthesis method and properties of some Garnets

Composition	Synthesis method	Sintering temperature (°C)	σ (S cm^{-1}) /T (°C)	Ref.
$Li_7La_3Zr_2O_{12}$	Solid-state reaction	1,180	4.16×10^{-4}/RT	[163]
$Li_7La_3Zr_2O_{12}$	Sol-gel processing	1,100	3.5×10^{-6}/30	[164]
$Li_{6.46}La_{2.94}Ba_{0.06}Zr_{1.4}Ta_{0.6}O_{12}$	Solid-state reaction	1,230	6.04×10^{-4}/30	[165]
$Li_{6.5}La_3Zr_{1.75}Te_{0.25}O_{12}$	Solid-state reaction	1,150	4×10^{-4}/RT	[166]
$Li_{6.4}La_3Zr_{1.7}W_{0.3}O_{12}$	Solid-state reaction	1,100	7.89×10^{-4}/30	[167]
$Li_{6.4}Ga_{0.2}La_{2.75}Y_{0.25}Zr_2O_{12}$	Solid-state reaction	900	1.6×10^{-3}/30	[168]
$Li_{6.6}La_3Zr_{1.6}Sb_{0.4}O_{12}$	Solid-state reaction	1,100	7.7×10^{-4}/30	[169]
$Li_{6.6}Al_{0.05}La_3Zr_{1.75}Nb_{0.25}O_{12}$	Sol-gel processing	1,150	6.3×10^{-4}/RT	[170]
$Li_7Al_{0.1}La_3Zr_2O_{12}$	Spark plasma sintering	1,000	8.8×10^{-4}/RT	[171]
$Li_{6.4}La_3Zr_{1.4}Ta_{0.6}O_{12}$	Spark plasma sintering	1,100	1×10^{-3}/RT	[172]

an ionic conductivity of 8.7×10^{-4} S cm^{-1} at 60 °C. This was ascribed to the ability of β-CDTFSI to significantly diminish the surface energy of LLZTO nanoparticles, which allowed LLZTO to be more uniformly dispersed in PEO. Moreover, β-CDTFSI with a unique cavity structure constructed a new lithium-ion channel between PEO and LLZTO, as shown in Figure 6E; the lithium-ion transport channel transitioned from the PEO matrix to LLZTO and subsequently back to PEO, resulting in a lithium-ion transference number of 0.48.

Huo *et al.* added 20 and 80 wt.% LLZTO to PEO, respectively, to investigate the impact of filler concentration on CSSEs[177]. With the increase in filler concentration, the ionic conductivity of electrolyte films decreased from 1.6×10^{-4} to 3.2×10^{-5} S cm^{-1} due to the transport channel of Li ions from migrating along the PEO-LLZTO interface to dispersed LLZTO interparticle migration. However, the tensile strength of the CSSE was elevated from 4.3 to 11.6 MPa. The influencing factors of mechanical properties mainly lie in the concentration of inorganic fillers and the degree of bonding with polymers. Generally, an increase in filler concentration enhances the strength of CSSEs; however, due to a low bonding degree between filler and polymer, a high filler content may promote polymer fluidity and consequently reduce the tensile strength of CSSEs[178].

In addition to its use as a polymer filler, many studies have shown that the use of LLZO directly as an electrolyte layer is compatible with electrodes. Nonetheless, a significant challenge in LLZO electrolytes is the elevated resistance at the electrode/electrolyte contact, attributed to the formation of a Li_2CO_3 layer on the electrolyte's surface. The interfacial layer obstructs the movement of Li ions at the electrode/electrolyte interface, resulting in unequal current distribution and ultimately promoting the formation of lithium dendrites.

NASICON type fillers

NASICON electrolytes were first called sodium superionic conductors, and their general chemical formula is $AM_2(PO_4)_3$. Alkali metal ions (Li^+, Na^+, K^+) are generally used at the A-site to transport cations. According to the elements in the M-site, NASICON electrolytes can be classified into three main types: $LiZr_2(PO_4)_3$ (LZP), $LiTi_2(PO_4)_3$ (LTP), and $LiGe(PO_4)_3$ (LGP). NASICON consists of PO_4 tetrahedra and MO_6 octahedra, as shown in Figure 6F; the upper oxygen atoms are bonded to two MO_6 octahedra and three PO_4 tetrahedra, with Li ions located in the M1, M2, and M3 locations, respectively, which together form a three-dimensional lithium-ion channel[179,180]. It has been found that the use of Al^{3+} with a smaller radius to replace the M-site ions can not only increase the lithium-ion concentration but also reduce the unit size of the crystal, thereby shortening the lithium-ion transport distance, which will make the electrolyte structure

more compact and improve the lithium-ion transport. Therefore, the research on NASICON-type electrolytes in recent years has mainly focused on $Li_{1+x}Al_xGe_{2-x}(PO_4)_3$ (LAGP) and $Li_{1+x}Al_xTi_{2-x}(PO_4)_3$. When the Al^{3+} content is low ($x < 0.2$), the excess Li ions tend to be trapped near Al^{3+}, which leads to higher grain boundary (GB) resistance and lower ionic conductivity[181]. In turn, when the Al^{3+} content is too much ($x > 0.7$), the formation of non-Li ions conducting the $AlPO_4$ phase near the GBs will also be unfavorable to the ionic conductivity, and in general, the optimum Al^{3+} content is considered to be around 0.3-0.5. It has been pointed out that the ionic conductivity of LATP and LAGP is related to the inhomogeneous phase of Al in their crystals; as shown in Figure 6G, LATP and LAGP have uniformly distributed Al/Li phases and exhibit good ionic conductivity when x is 0.4 and 0.5, respectively[182]. Table 4 shows the crystal synthesis method and properties of some NASICONs.

The LATP and LAGP electrolytes exhibit elevated room-temperature ionic conductivity and commendable chemical stability, and high oxidation voltages (6 V), among other advantages, and they are inexpensive. Compared to other electrolytes, the excellent high stability of LATP and LAGP to H_2O and CO_2 allows for stable preparation and use in air. However, side reactions occur when they come into contact with the lithium anode; Ti^{4+} in LATP-type electrolytes is reduced to Ti^{3+}, and Ge^{4+} in LAGP-type electrolytes is reduced to Ge^{2+} and Ge^0, resulting in a severe increase in the resistance at the interface until the battery fails[193,194]. Therefore, LATP and LAGP are often not directly matched with electrode materials to be assembled into lithium-ion batteries but must be treated at the interface or combined with polymer electrolytes.

Sun *et al.* prepared $Li_{1.5}Al_{0.5}Ge_{1.5}(PO_4)_3$, using the lower-cost inorganic germanium (GeO_2) as a precursor by sol-gel method[195]. The highest ionic conductivity of the LAGP samples prepared by sintering at 900 °C for 8 h reached 7.76×10^{-4} S cm^{-1}. Huang *et al.* prepared electrolyte films by filling the LAGP with Polyphenylene Oxide (PPO) and transformed ceramic-in-polymer into polymer-in-ceramic by modulating the dosage of LAGP[196]. The electrolyte prepared by filling 75% LAGP has an ionic conductivity of 3.46×10^{-4} S cm^{-1}, lithium-ion transference number of 0.83, a voltage stability window of 4.78 V. As shown in Figure 6H, the PPO-75% LAGP electrolyte film can remain stable at high temperatures, implying that it can work stably at high temperatures.

Doping metal atoms is a common technique to enhance the ionic conductivity of NASICON electrolytes. Panda *et al.* prepared LATP electrolytes doped with cobalt and copper (Co-LATP and Cu-LATP), respectively[197]. Both Cu and Co can reduce the grain size, and the resultant GBs facilitate the migration of Li ions in LATP, enhancing ionic conductivity. After the two LATP electrolytes were prepared into CSSE films with PVDF-HFP and LiTFSI, the highest ionic conductivity at room temperature was 3.18×10^{-4} S cm^{-1} (Co-LATP) and 2.99×10^{-4} S cm^{-1} (Cu-LATP), respectively.

It has been found that modulating the morphology and arrangement of LATP can improve the ionic conductivity of CSSEs. Lu *et al.* prepared LATP with microporous channels (p-LATP) using polyethylene-polypropylene glycol F127 as a template, and this long-range ordered tubular pore allows for the rapid transport of Li ions[198]. p-LATP with a filling amount of 40 wt.% of the ionic conductivity of the prepared PEO-p-LATP electrolyte was 3.5×10^{-4} S cm^{-1}. Moreover, the ionic conductivity may be further improved by combining p-LATP with standard dense LATP using microporous channels and dense lithium-ion conductive areas.

The primary issue constraining the utilization of LLZO and LATP electrolytes is the side reaction occurring between them and the lithium metal contact. Although the existence of a polymer matrix has alleviated this

Table 4. The crystal synthesis method and properties of some NASICONs

Composition	Synthesis method	Sintering temperature (°C)	σ (S cm^{-1})/T (°C)	Ref.
$Li_{1.4}Al_{0.4}Ti_{1.6}(PO_4)_3$	Co-precipitation	900	1.8×10^{-4}/RT	[183]
$Li_{1.3}Al_{0.3}Ti_{1.7}(PO_4)_3$	Sol-gel processing	900	1.2×10^{-4}/RT	[184]
$Li_{1.3}Al_{0.3}Ti_{1.7}(PO_4)_3$	Mechanical activation	900	6.2×10^{-5}/25	[185]
$Li_{1.5}Al_{0.5}Ti_{1.5}(PO_4)_3$	Sol-gel processing	1,000	4.5×10^{-4}/30	[186]
$Li_{1.3}Al_{0.3}Sn_{0.35}Ti_{1.35}(PO_4)_3$	Solid-state reaction	900	4.7×10^{-4}/RT	[187]
$Li_{1.5}Al_{0.5}Ge_{1.5}(PO_4)_3$	Cold sintering processing	120	5.4×10^{-5}/25	[188]
$Li_{1.5}Al_{0.5}Ge_{1.5}(PO_4)_3$	Hot-pressing	550	1.8×10^{-4}/RT	[189]
$Li_{1.5}Al_{0.5}Ge_{1.5}(PO_4)_3$	Sol-gel processing	850	3.1×10^{-4}/30	[190]
$Li_{1.5}Al_{0.5}Ge_{1.5}(PO_4)_3$	Spark plasma sintering	950	1.3×10^{-4}/20	[191]
$Li_{1.5}Al_{0.3}B_{0.1}Ga_{0.1}Ge_{1.5}(PO_4)_3$	Microwave sintering	900	3.8×10^{-4}/RT	[192]

problem to a large extent, there is still no complete solution. At the same time, the morphology and arrangement of the two compounds in the polymer greatly influence the properties of CSSEs, and advanced synthesis methods are needed to obtain materials with uniform properties.

STRUCTURE DESIGN OF FILLERS IN CSSES

Filler particles have a substantial specific surface area, enabling them to effectively inhibit crystal formation in polymers and enhance the mobility of Li ions in the electrolyte. Even though Li ions can be conducted inside the active filler, agglomerating and caking problems still lead to a decrease in ionic conductivity[199]. Therefore, many scholars have started to make more structural designs for CSSEs: 1D nanowires/nanofibers, and 2D flakes[200].

1D fillers

For inert fillers, due to the agglomeration of nanoparticles and non-ionic conductivity, the content of inert fillers should be manageable. Otherwise, it will rather reduce the ionic conductivity of the electrolyte. In this case, using 1D fillers can not only slow down the agglomeration problem, but also, 1D inert fillers have longer dimensions, providing a more continuous lithium-ion transport channel. TiO_2 is a relatively joint 1D inert filler. As shown in Figure 7A, the filling of nanowires can provide more rapid lithium-ion channels[201]. Hua *et al.* filled the TiO_2 nanorods into the poly(propylene carbonate) (PPC), the utilization of rod-shaped materials rather than randomly dispersed particles to establish a continuous transport channel for Li ions, the preparation of CSSE with an electrochemical window of 4.6 V and an ionic conductivity of 1.52×10^{-4} S cm^{-1} at room temperature[202]. Luo *et al.* fabricated TiO_2 micro-rods with a high concentration of oxygen vacancies[203]. These vacancies not only decreased the crystallinity of the polymers but also facilitated the dissociation of LiTFSI by interacting with the -CF_3 group of the $TFSI^-$ on the surface of the TiO_2 microrod. The preparation process is shown in Figure 7B. The ionic conductivity reached 1.04×10^{-4} S cm^{-1} at room temperature.

The MOF material can additionally be synthesized as a 1D nanowire to integrate into the polymer electrolyte matrix. Xu *et al.* designed a colloidally dispersed nonporous MOF (Bi/HMT-MOF) nanowire with a shallow surface area using Bi^{3+} as the metal center[204]. The preparation process is shown in Figure 7C. The 1D structure enables Bi/HMT-MOF to have better compatibility with PEO. Bi^{3+} facilitates the dissociation of lithium salts and interacts with EO to form an amorphous PEO interfacial layer on the nanowire surface, enhancing the fast transport of Li ions. The prepared CSSE has a conductivity of 5.89×10^{-4} S cm^{-1} at 60 °C.

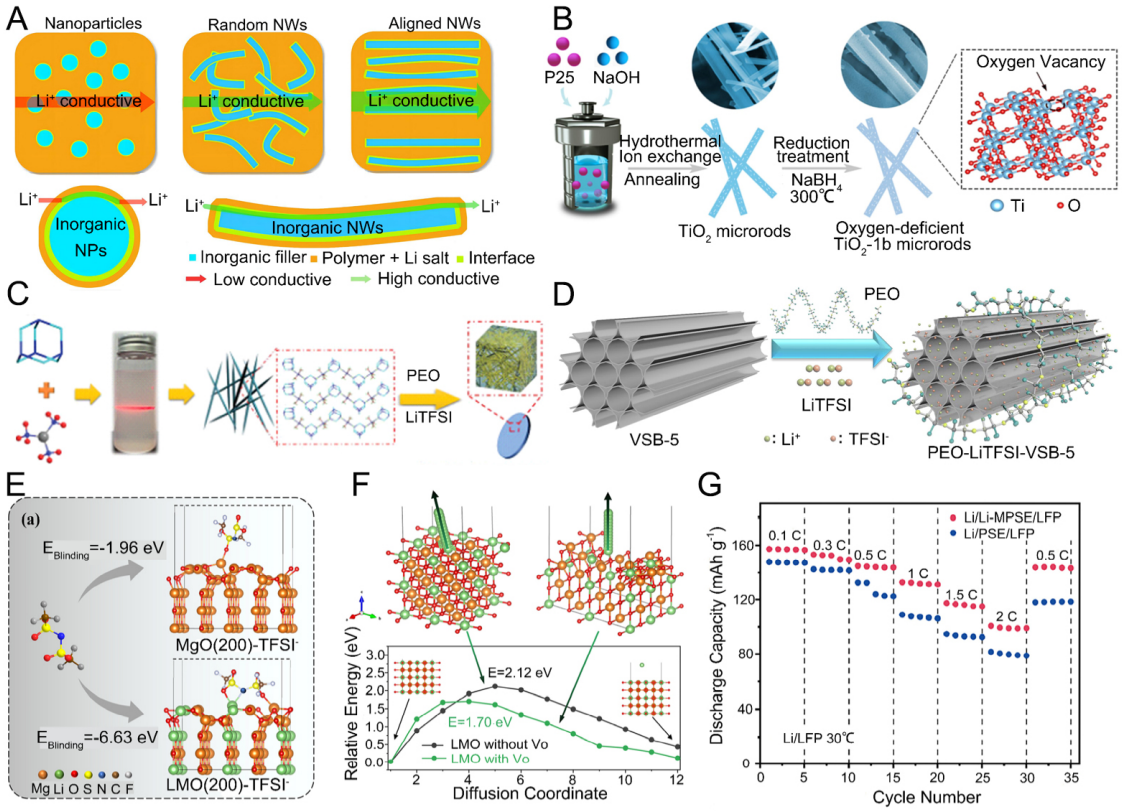

Figure 7. Schematic illustration of (A) nanowires providing fast lithium-ion channels[201]. Reproduced from Ref.[201] with permission. Copyright 2017, Nature. (B) The preparation of TiO_2 nanorods enriched with oxygen vacancies[201]. Reproduced from Ref.[203] with permission. Copyright 2022, Elsevier. (C) The preparation of Bi/HMT-MOFs nanowire and BMCPE film[204]. Reproduced from Ref.[204] with permission. Copyright 2022, Wiley-VCH. (D) Lithium-ion migration in VSB-5 enhanced PEO electrolytes[205]. Reproduced from Ref.[205] with permission. Copyright 2020, Elsevier. (E) A side view of the LiTFSI crystal structure derived from DFT calculations is adsorbed on the surface of MgO (200) and LMO (200), containing one oxygen vacancy. (F) Channels of a single Li ion severed from the LMO lattice, depicted without (left) and with (right) an oxygen vacancy[206]. Reproduced from Ref.[206] with permission. Copyright 2023, American Chemical Society. (G) Evaluate the performance of Li|Li-MPSE|LFP battery and Li|PSE|LFP battery at a discharge rate of 0.5 C at 30 °C[207]. Reproduced from Ref.[207] with permission. Copyright 2023, Elsevier.

Besides conventional nanofillers such as metal oxides, materials featuring 1D channels can also be utilized to enhance polymer electrolytes. Wu *et al.* used nickel phosphonate VSB-5 as a filler for PEO, which not only reduces the crystallinity of PEO, as shown in Figure 7D, but also has its large pore size of 1.1 nm 1D channels[205]. When the amount of VSB-5 was 3 wt.%, the prepared PEO-LiTFSI-3 wt.% VSB-5 had an ionic conductivity of 4.83×10^{-5} S cm^{-1} at 30 °C. Furthermore, the incorporation of VSB-5 into the CSSE enhances its thermal stability and electrochemical stability window (4.13 V) compared to the pure PEO electrolyte. Furthermore, it enhances the inhibition of lithium dendrite development.

Similar to nanoparticles, the diffusion kinetics of Li ions can be effectively improved by rational surface defect design of 1D oxide nanofillers. Positively charged oxygen vacancies represent the predominant surface defect configuration, achievable by substituting high-valent elements with those of lower valence. This surface imperfection primarily enhances the ionic conductivity of electrolytes by facilitating the dissociation of lithium salts, hence releasing a greater quantity of Li ions. Yu *et al.* prepared lithium-doped MgO (LMO) nanofibers by using electrostatic spinning and calcination, and after compositing them with PEO/LiTFSI, the inorganic filler with 1D morphology firstly reduces the crystallinity of the polymer and provides a continuous Li transport channel[206]. In addition, lithium doping can introduce many positively

charged oxygen vacancies in the lattice structure, enabling LMO to adsorb more anions from Li salts and thus release more Li ions. As shown in Figure 7E, when Li is immobilized in MgO, supplementary Li-N and Li-O bonds can be established, resulting in an adsorption energy of $TFSI^-$ at -6.63 eV, which signifies an enhancement in the obstruction of free $TFSI^-$. The potential barriers required for Li to spill out of the lattice are about 2.12 and 1.70 eV for LMOs with and without oxygen vacancies, respectively, as shown in Figure 7F. This indicates that flaws or compromised chemical bonds may promote the movement of Li ions adjacent to oxygen vacancies, enabling them to surmount the energy barrier and exit the lattice. In addition to utilizing 1D morphology fillers, constructing vertically oriented 1D Li ion channels can achieve the same effect. Wang *et al.* designed a CSSE with vertically aligned 1D lithium-ion transport channels[207]. Lithium MMT is embedded in PVDF-HFP along a 1D vertically aligned channel to prepare a CSSE (Li-MPSE), which provides a one-dimensional efficient transport channel for Li ions. At the same time, the Li dissolution environment in the vinyl carbonate-based electrolyte was altered to establish the lithium-ion hopping pathway. This CSSE has an ionic conductivity of 1.99×10^{-4} S cm^{-1} and a lithium-ion transference number of 0.73. The rate performance test further demonstrates the superiority of Li-MPSE, as shown in Figure 7G.

When the polymer electrolyte matrix is filled with active fillers, Li ions are more inclined to be transported at the polymer/particle interface. Therefore, when the active fillers are designed as a 1D structure, the number of lithium-ion migrations between multiple filler particles can be reduced so that Li ions can be transported along the 1D active filler in a long-range and rapid manner, improving the ionic conductivity of CSSEs[208]. In general, active fillers often require electrostatic spinning to prepare nanowires with fiber networks, followed by high-temperature sintering to obtain 1D active filler nanorods.

Zhu *et al.* prepared LLTO nanowires (LLTO NWs) using electrostatic spinning and high-temperature sintering, which were filled into PEO to prepare CSSEs[209]. The ionic conductivity of the CSSE is 5.53×10^{-5} and 3.63×10^{-4} S cm^{-1} at room temperature and 60 °C, respectively, when the amount of LLTO was 5 wt.%. Figure 8A shows the LLTO NWs prepared by electrostatic spinning, and the results show that these NWs have a diameter of about 1 μm and can be dispersed uniformly into the PEO matrix. As shown in Figure 8B, the assembled Li|CSSE|LFP battery exhibits good specific capacity and capacity retention at 0.5 C. Bi *et al.* took the prepared LLTO NWs and prepared PAN/SEO by using a second utilization of the PAN/SN/LLTO CSSE film prepared by electrostatic spinning[210]. This CSSE film can exhibit an ionic conductivity of up to 2.2×10^{-3} S cm^{-1} at 30 °C and a broad electrochemical window of 5.1 V. In addition to LLTO-type electrolytes, garnet-structured LLZO electrolytes are often prepared as 1D structures to improve the performance of CSSEs. Li *et al.* also prepared LLZO nanofiber materials using electrostatic spinning and sintering processes, which were added to PVDF-HFP/LiTFSI to prepare a CSSE film[211]. The CSSE containing 10 wt.% of LLZO was found to have an ionic conductivity of 9.5×10^{-4} S cm^{-1} at 20 °C. The assembled Li|PVDF-HFP/LiTFSI/LLTO|LFP battery can be stabilized with 140 mAh g^{-1} capacity at 0.2 C for 120 cycles.

Cation doping techniques have also been applied in the design of nanowires, where the dissociation of lithium salts by active fillers can be enhanced by different cation doping, increasing the lithium-ion concentration in CSSEs. Sun *et al.* designed Nb-doped $Li_{6.75}La_3Zr_{1.75}Nb_{0.25}O_{12}$ (LLZNO) nanowires[212], which were blended with PMMA and $LiClO_4$ to prepare a CSSE with an ionic conductivity of 2.20×10^{-5} S cm^{-1}. Figure 8C illustrates the ionic transport channel within the prepared electrolyte, wherein a greater number of Li ions are dissociated through interaction with the anion. Ding *et al.* designed a tantalum-aluminum co-substituted LLZO nanowire electrolyte, which not only provides long-range interfaces to improve ionic conductivity but also has more lithium vacancies to further promote Lewis acid-base interaction of the

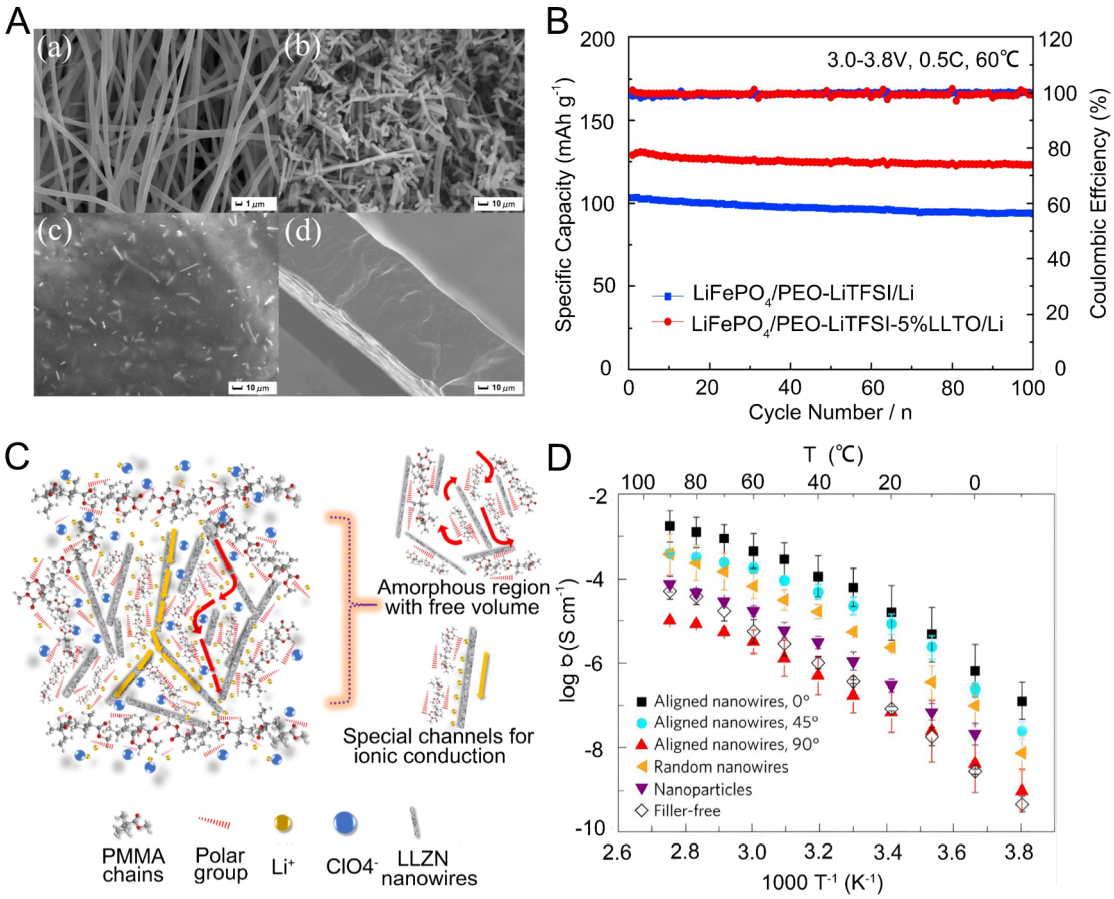

Figure 8. (A) Images of LLTO nanowires prepared by electrostatic spinning, surface, and cross-section images of prepared CSSE films. (B) Cycling performance of Li|PEO/5% LLTO NWs|LFP battery at 0.5 C[209]. Reproduced from Ref.[209] with permission. Copyright 2022, Elsevier. (C) Schematic illustration of ionic transport mechanisms in CSSEs with 10 wt.% LLZN nanowires[212]. Reproduced from Ref.[212] with permission. Copyright 2018, Elsevier. (D) Ionic conductivity plots of CSSEs with randomly oriented nanowires and nanowires arranged in different directions[201]. Reproduced from Ref.[201] with permission. Copyright 2017, Nature.

electrolyte with lithium salts[213]. The CSSE, formulated using the PEO matrix, exhibits a lithium-ion transference number of 0.79 and an ionic conductivity of 3.8×10^{-4} S cm^{-1}.

Furthermore, it has been noted that well-aligned nanowires can enhance the performance of the CSSE more effectively than a randomly oriented distribution of nanowires. Liu *et al.* prepared CSSEs filled with randomly oriented LLTO NWs and CSSEs with oriented aligned LLTO NWs, by using PAN as the matrix[201]. As shown in Figure 8D, the electrolyte with randomly dispersed nanowire fillers had an ionic conductivity of 5.40×10^{-6} S cm^{-1} at 3 wt.% filler and 30 °C, while the electrolyte containing well-aligned nanowires exhibited an ionic conductivity of 6.05×10^{-5} S cm^{-1}. Compared to nanoparticles, nanowires provide a more continuous interface for Li ion transport, and well-aligned nanowires can transport Li ions faster than randomly aligned nanowires due to the absence of surface crossings.

2D fillers

To improve the ionic conductivity of the CSSEs, the contact area between the inert fillers and the interface may be augmented. This is because the fillers themselves are unable to transport Li ions, and instead depend on the filler/interface to create a channel for lithium-ion transport. Therefore, compared to 0D and 1D inert

fillers, 2D fillers with a layered structure become a better choice[214,215]. The design of 2D fillers significantly enhances the contact area between the polymer and the filler. Moreover, 0D and 1D fillers produce a part of unwanted volume due to their inability to transport Li ions within themselves, which is unfavorable to ionic conductivity. At the same time, the laminated 2D material reduces this part of unwanted volume very well[216,217]. However, the disadvantages of 2D materials are also apparent, as they are prone to curling and aggregation when dispersed in a polymer matrix, which makes it challenging to take advantage of their high specific surface area. Simultaneously, the 2D material has a distribution direction that is perpendicular to the direction of lithium-ion transport. This perpendicular distribution is predicted to impede the passage of Li ions between the electrodes.

Sun *et al.* prepared CSSE by mixing g-C_3N_4 nanosheets with PEO and LiTFSI for the first time[218]. The 2D configuration of g-C_3N_4 was utilized to create an expanded lithium-ion transport region, hence enhancing ionic conductivity. As the surface of g-C_3N_4 is rich in N atoms, it can better dissociate the lithium salts in the CSSE at 30 °C, the ionic conductivity of the prepared CSSE is 1.7×10^{-5} S cm^{-1}, and the lithium-ion transference number reaches 0.56. Silicates are natural ore materials with a 2D layered structure. Zhao *et al.* used *in situ* polymerization of allyl acetoacetate (AAA) monomers to prepare LPAS electrolyte films containing SiO_2 nanosheets with oxygen vacancies, and the structure of LPAS is shown in Figure 9A[51]. The SiO_2 nanosheets can dissociate LiTFSI by immobilizing the anions. The presence of the oxygen vacancies accelerates the migration of Li ions, which results in the LPAS having a 3.82×10^{-4} S cm^{-1} ionic conductivity and 0.66 lithium-ion transference number. Moreover, the 2D structure of SiO_2 forms an intercalation network in PMMA, which reduces the crystallinity while maintaining good viscoelasticity. Wu *et al.* incorporated 15 wt.% of 2D $MoSe_2$ sheets into PVDF to develop an electrolyte (PVVMS-15) in which positively charged Mo atoms and negatively charged Se atoms interact with -CF_2- and -CH_2-, respectively[219]. This interaction enables the conversion of PVDF into the all-trans (β-phase), optimizing the solvation structure and resulting in an ionic conductivity of PVVMS-15 reaching 6.5×10^{-4} S cm^{-1}.

MOF and covalent organic frameworks (COFs) materials can perform better when they are designed as 2D fillers. By molecular engineering, Xu *et al.* designed a 2D MOF sheet rich in -NH_2 on the surface. The substituents in this MOF material enhanced the electron-donating effect[220]. When compounded with PEO and $LiClO_4$ to prepare an electrolyte, it could better restrict the movement of ClO^{4-} thus increasing the lithium-ion transference number to 0.64. This electrolyte achieved an ionic conductivity of 6.5×10^{-5} S cm^{-1} at room temperature. Saleem *et al.* incorporated 2D pyrazine and imine-linked COFs into a PEO electrolyte matrix[221]. The distinctive amalgamation of electron-rich and polar functions in the COFs facilitates strong interactions with Li ions, yielding an ionic conductivity of 1.86×10^{-3} S cm^{-1} at ambient temperature. Furthermore, the prepared electrolyte film exhibits excellent flexibility and fully recovers after undergoing 360° folding, effectively mitigating the growth of lithium dendrites and interface instability.

MXene, a category of 2D transition metal carbides, is utilized in CSSEs because of its distinctive electrical and mechanical characteristics. Zhao *et al.* designed Li anodic interfacial layers using silk fibroin peptide (SFP), acetylene black (AB), and MXene and applied them to the LOPPM prepared in their previous work[222]. As shown in Figure 9B, the formation of LiN_3 and LiF was successfully promoted by utilizing the -NH_2 group in SFP combined with -F in MXene. This work realized the *in-situ* formation of uniform SEI membranes and effectively suppressed the growth of lithium dendrites. In their other work, LiTFSI/OMMT/soybean isolate protein (SPI)/PVDF (LOSP) electrolytes were prepared, and the above interface design was applied to LOSP[223]. As shown in Figure 9C, spherical lithium deposition was achieved at the electrolyte/electrode interface, forming a stable interfacial layer that can promote the reversible transport of Li ions. Molybdenum carbide (Mo_2C) reduces the lithium-ion transfer energy barrier and is also often used

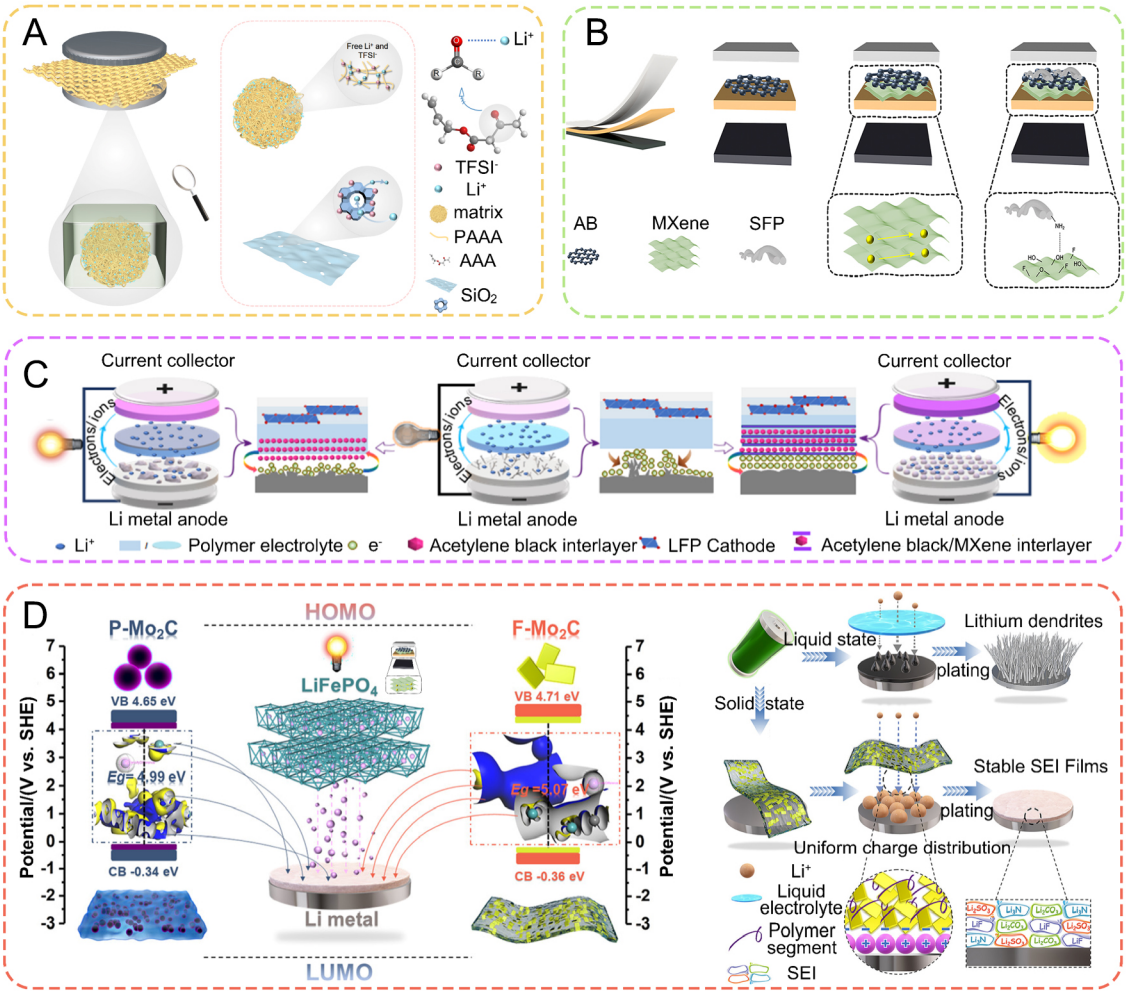

Figure 9. (A) Schematic illustration of LPAS SPE[51]. Reproduced from Ref.[51] with permission. Copyright 2024, Wiley-VCH. (B) Schematic illustration of the interaction between MXene and SFP[222]. Reproduced from Ref.[222] with permission. Copyright 2023, Elsevier. (C) Schematic representation of interface change in a charge equalizer resulting in spherical lithium deposition for batteries[223]. Reproduced from Ref.[223] with permission. Copyright 2023, Wiley-VCH. (D) Schematic illustration of LFCPP, LPCPP electrolytes, and lithium deposition mechanism promoted by LFCPP[224]. Reproduced from Ref.[224] with permission. Copyright 2022, American Chemical Society.

to improve electrode/electrolyte interface problems. Shan *et al.* designed LiTFSI/nanosheet Mo_2C (F-Mo_2C)/PVDF/PVDF-HFP electrolyte (LFCPP) and LiTFSI/nanoparticle Mo_2C (P-Mo_2C)/PVDF/PVDF-HFP (LPCPP)[224]. This study illustrates that F-Mo_2C can create unique charge channels that enhance the uniform deposition of lithium particles, and Figure 9D shows the schematic illustration of the two electrolytes and the LFCPP to promote lithium deposition.

Compared to inert fillers, there has been less research on 2D active fillers. One possible explanation is that the current manufacturing technology cannot produce significant amounts of active nanosheets. At present, the preparation methods involve the use of template and electrostatic spinning techniques. Liu *et al.* prepared 2D fibrous films filled with PEO by LLTO using electrostatic spinning and then coated with a layer of PEO on both sides of the fibrous films to prevent the LLTO from direct contact with the Li negative electrode to produce a reduction reaction[225]. In addition, the design of the PEO coating on both sides facilitates optimal interfacial contact between the electrolyte and the electrode, thereby greatly reducing

interfacial impedance. The ionic conductivity of this sandwich CSSE is 1.6×10^{-4} S cm^{-1} at room temperature.

Due to the process difficulty of 2D active fillers, most current research involves preparing micron-sized 2D materials using the press-sintering process and using them directly as electrolyte-matched electrodes to prepare LMBs[226]. Nonetheless, the contact between electrodes and electrolytes requires resolution[227,228]. Huang *et al.* solved the reduction reaction of LATP on a lithium-negative electrode by constructing a flexible buffer layer of PVDF and Mg_3N_2 particles on the surface of the LATP sheet[229]. This interfacial design constructed a multifunctional intermediate layer of Mg, LiF, and Li_3N *in situ* at the electrolyte/electrode interface, which inhibited the decomposition of LATP. It increased the critical current density of LATP from 0.34 to 0.76 mA cm^{-2}. Liu *et al.* prepared Ga-containing LLZO (Ga-LLZO) electrolytes, then incorporated ionic liquid into the Ga-LLZO electrolytes, and subsequently coated ionic liquid-containing PEO (IL-PEO) on the surface of Ga-LLZO electrolytes to improve the contact with the electrodes[230]. The IL-PEO coating, on the one hand, solves the rigidity problem of Ga-LLZO, which leads to a significant electrolyte/electrode impedance problem. On the other hand, it enhances the stability of LLZO electrolytes in humid air, diminishes the formation of the Li_2CO_3 phase, and increases ionic conductivity. The electrolyte with the coating attained an ionic conductivity of 5.7×10^{-4} S cm^{-1} at ambient temperature.

PREPARATION AND CHARACTERIZATION OF CSSES

Preparation method of fillers

There are many mature processes for the synthesis of fillers; the most commonly used methods are introduced here: hydrothermal reaction, solid-state reaction, and sol-gel processing. The hydrothermal method is often used to synthesize materials such as metal oxides and MOFs, and the advantage of the hydrothermal method is that it can form complex structures under relatively mild conditions. Generally, the appropriate raw material is selected according to the target product, and some auxiliary reagents are added after it is dissolved in water. It is then transferred to a high-pressure reactor, sealed, and heated in an oven between 100-300 °C, and the product can be obtained by natural cooling after the reaction[78].

Active fillers are frequently prepared using solid-state reaction processes and sol-gel processing techniques. The solid phase reaction method is the precursor powder according to the stoichiometric ratio after mechanical grinding mixed and calcined at the appropriate temperature to obtain the material[141]. The sol-gel processing method is the stoichiometric ratio of raw materials and metal salts dissolved in water or alcohol solvents by adding catalysts or adjusting the pH to promote a hydrolysis reaction to form a highly dispersed suspension (sol). When the particles in the sol are further cross-linked, a three-dimensional network structure (gel) is synthesized, subsequently dried, and calcined to yield the material[142].

Preparation method of CSSEs

The most straightforward approach for preparing CSSEs is solution blending, as shown in Figure 10A, in which the polymer matrix and filler are dissolved and agitated in an organic solvent to attain uniform dispersion before being formed into an electrolyte film[231]. Alternatively, melt blending disperses the filler in the molten polymer matrix to prepare the electrolyte film, offering the advantage of avoiding solvent residue compared to solution blending[232]. Powder blending involves mixing polymer powder and fillers, followed by grinding and hot pressing to prepare the electrolyte film[233]. This approach can mitigate strong shear forces during melt blending, hence maintaining the mechanical integrity of the electrolyte film to prevent polymer chain rupture. In addition to direct blending, *in-situ* polymerization is also utilized for CSSE preparation. The general process involves dissolving polymer monomers, initiators, fillers, and lithium salt in a suitable solvent before casting onto electrodes and solidifying using ultraviolet or thermal

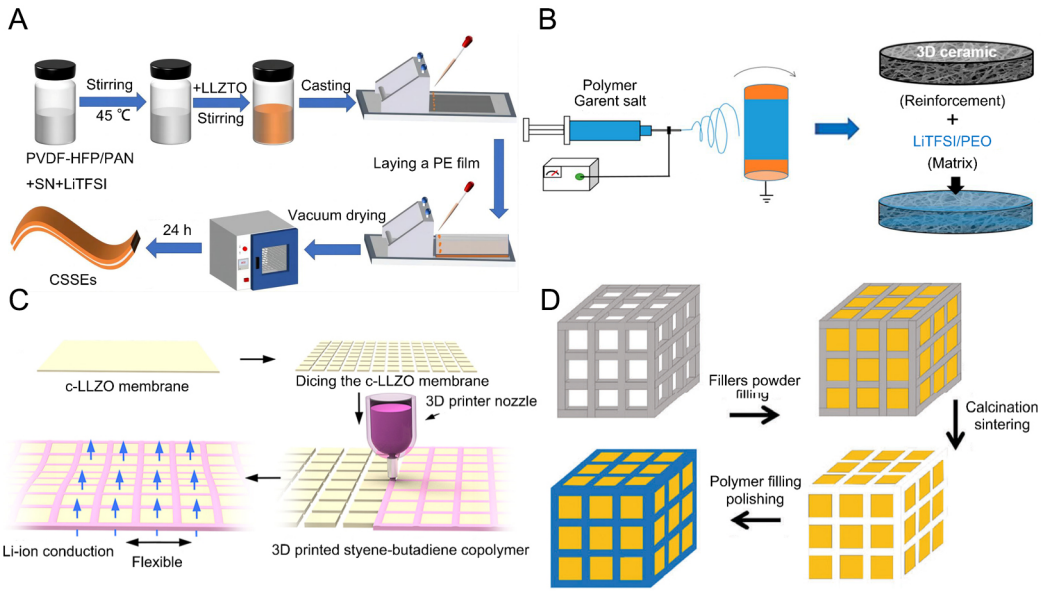

Figure 10. CSSEs preparation method (A) Solution casting method[231]. Reproduced from Ref.[231] with permission. Copyright 2022 Springer Nature. (B) Electrostatic spinning method[95]. Reproduced from Ref.[95] with permission. Copyright 2016, PNAS. (C) 3D printing method[235]. Reproduced from Ref.[237] with permission. Copyright 2019, American Chemical Society. (D) Template method[238]. Reproduced from Ref.[238] with permission. Copyright 2018, Royal Society of Chemistry.

initiation[234,235]. While this method effectively addresses electrode/electrolyte interface contact issues, it may result in significant solvent residues.

In addition to the above methods, there are several techniques for building CSSEs with 3D frame structures. Examples include the electrostatic spinning method, 3D printing method, and template method. An excellent advantage of these methods is the continuous structure in CSSEs. As shown in Figure 10B, the electrostatic spinning method utilizes a DC high-voltage power supply to mix the electrolyte solution in a syringe to form nanofibers on the collector[95]. After the solvent is removed, an electrolyte film is obtained. The 3D printing technology can efficiently investigate structure-property relationships, allowing for rapid exploration and analysis[236]. This method uses extruded polymer adhesives to join multiple filler sheets [Figure 10C] and the prepared CSSEs have extremely high flexibility and can reduce strain during the use of the material[237]. The template method generally adds the filler to the template first [Figure 10D], then makes the filler have a special structure by sintering and removing the template, and finally infuses the polymer matrix into the filler structure[238]. Table 5 provides an overview of the advantages and disadvantages of general synthesis methods for CSSEs. Despite the availability of these more mature techniques, it is still a challenge to customize 3D frames with highly ordered structures accurately.

These structural designs augment the interface between fillers and polymers, facilitating continuous transport channels for lithium-ion migration while maintaining low concentration, thereby contributing to improved ionic conductivity of CSSEs. The construction of a continuous lithium-ion transport channel by active fillers within the 3D framework design further enhances ionic conductivity. However, the insulation properties of inert filler to Li ions may lead to a significant reduction in ionic conductivity if a continuous 3D structure of inert filler skeleton is constructed, resulting in a large volume ratio of lithium insulation region in the polymer matrix. As such, there are few discussions in the literature on 3D structural design for inert fillers.

Table 5. Some preparation methods of CSSEs and their advantages and disadvantages

Preparation method	Advantage	Disadvantage
Solution blending	Simple process High uniformity	Residual solvent Low mechanical strength
Melt blending	Solvent-free	High-temperature decomposition Poor uniformity
Powder blending	Solvent-free High mechanical strength	Poor uniformity
In-situ polymerization	Tight electrode/electrolyte interface	Residual solvent
Electrospinning method	High mechanical strength High ionic conductivity	Low efficiency
Template method	High mechanical strength High ionic conductivity	Template removal problem

Advanced characterization of CSSEs

Morphology characterization technique

Scanning electron microscopy (SEM) is a widely used technology for the characterization of microscopic morphology in materials science. In addition to imaging microscopic morphology, SEM-based energy spectrum technologies, such as energy dispersive energy spectrometers (EDS), can provide quantitative analysis of the local element composition of materials, reflecting the dispersion degree of fillers in polymer matrix to a certain extent[239]. The atomic force microscope (AFM) enables the characterization of material morphology at nanoscale resolution and the direct characterization of insulating materials. Furthermore, AFM can be utilized for imaging in various environments. It is capable of characterizing changes in the morphology and mechanical properties of electrolytes at different temperatures; for example, Figure 11A demonstrates the characterization of the morphology, Young's modulus, and adhesion of PEO/$LiClO_4$ electrolyte at 30 and 55 °C using *in-situ* c-AFM[240]. When lithium deposition is observed within CSSEs by SEM, corrosion occurs during the sample transfer. This challenge can be addressed through *in situ* optical microscopy, enabling the observation of CSSE behavior during electrochemical reactions in a specific environment. As depicted in Figure 11B-D, cross-sectional snapshots of Li/Li_3PS_4/NCM battery charging are characterized using *in situ* optical microscopy[241].

Moreover, cryopreservation high-resolution transmission electron microscopy (cryo-HRTEM) can provide detailed characterization of structural features within CSSEs, such as nanoscale structure and GB characteristics. Rapidly cooling and freezing CSSEs can help material avoid changes at room temperature. As illustrated in Figure 11E and F, cryo-HRTEM allows for the characterization of LLZO grains and the nanoscale region of GBs, with corresponding Fast Fourier transform (FFT) diagrams [Figure 11G] providing clear insights[242].

Component characterization technique

Fourier Transform Infrared spectroscopy (FTIR) is a vibrational spectroscopy technique widely employed to study functional groups and chemical structures in organic molecules. The interaction within the polymer can be obtained by FTIR analysis of CSSEs to analyze the properties change before and after adding fillers[243]. X-ray photoelectron spectroscopy (XPS) can accurately and qualitatively analyze the types of elements on the material surface to determine the relative content of elements according to the peak intensity. Secondary Ion Mass Spectrometry (SIMS) is a precise surface analysis method that generates secondary ions by the bombardment of a sample's surface, which are subsequently collected and evaluated using a mass spectrometer. The advantage of SIMS technology is that it can accurately locate the location and distribution of Li ions in the CSSEs, which can better evaluate the battery efficiency[244].

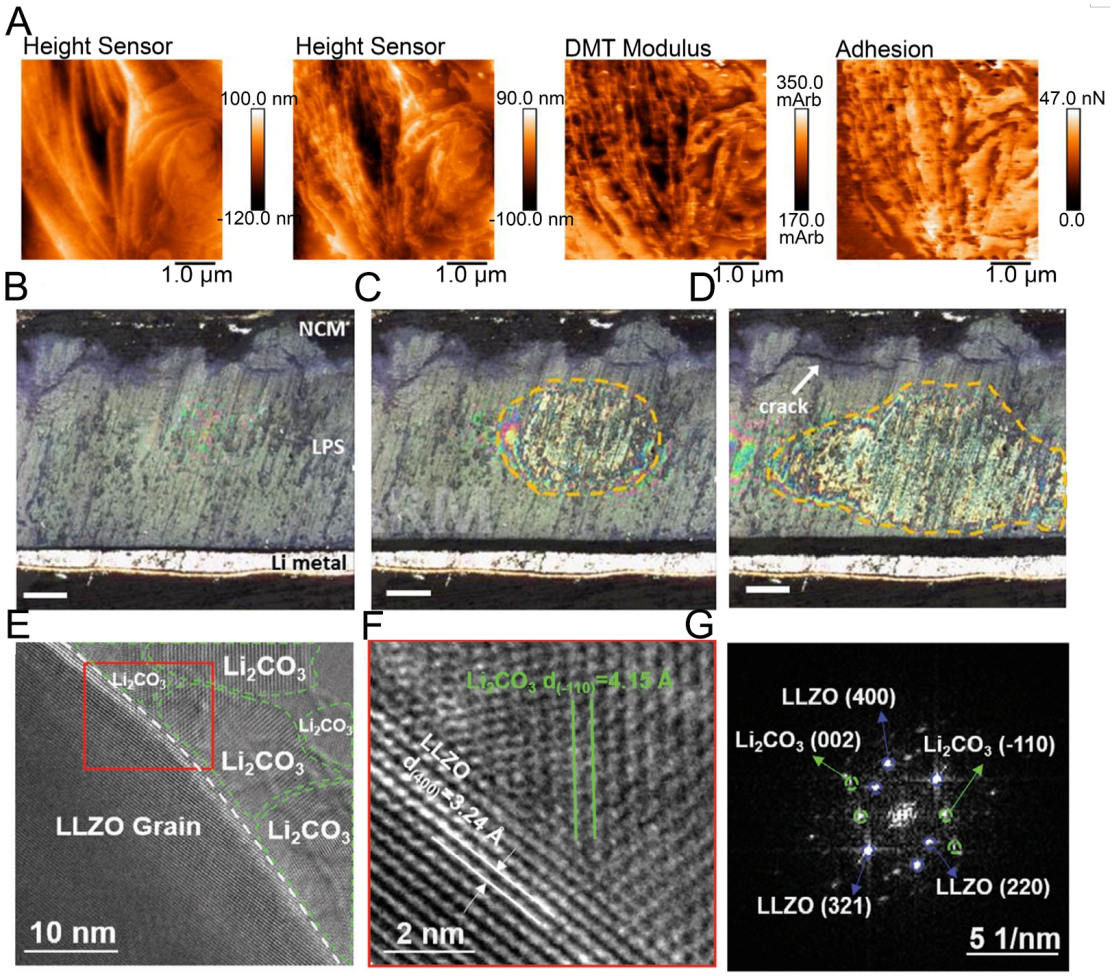

Figure 11. (A) *In situ* c-AFM characterization of the morphology, Young modulus and adhesion of PEO/$LiClO_4$ at 30 and 55 °C[240]. Reproduced from Ref.[240] with permission. Copyright 2021, Elsevier. Cross-sectional snapshots of Li/Li_3PS_4/NCM battery taken at 0 h (B), 6 h (C), and 18 h (D)[241]. Reproduced from Ref.[241] with permission. Copyright 2021, American Chemical Society (E) Cryo-HRTEM images of pristine LLZO grain and GBs. (F) Magnified cryo-HRTEM and (G) FFT images of the area within the red square in (E)[242]. Reproduced from Ref.[242] with permission. Copyright 2023, Wiley-VCH.

RELATIONSHIP BETWEEN FILLERS AND BATTERIES PERFORMANCE WITH CSSES

Improve battery cycle stability

The primary factor constraining the cycle stability of ASSLMBs is the proliferation of lithium dendrites. Despite the flexible polymer's ability to establish effective interface contact, it remains incapable of inhibiting the proliferation of lithium dendrites, hence diminishing battery longevity. The incorporation of fillers is anticipated to address this issue; fillers not only augment the mechanical strength of CSSEs to avert punctures from lithium dendrites, but numerous fillers can also establish a stable interfacial layer at the direct contact between lithium metal and electrolyte, thereby restricting the proliferation of lithium dendrites.

Li *et al.* added TiO_2 nanotubes to the PEO, and the prepared electrolyte formed a LiF-rich interface layer between the lithium metal and the electrolyte, achieving rapid lithium-ion transport and uniform lithium deposition[245]. The Li|PEO-TiO_2|LFP battery was cycled more than 3,100 times at 1 C, showing excellent cycle stability. Pang *et al.* prepared Ga/Ta co-doped LLZO and added it to PVDF to prepare an electrolyte [$PL(Ga_{0.1}Ta_{0.3})_{2.5}$]. $PL(Ga_{0.1}Ta_{0.3})_{2.5}$ has a polarization voltage of only 0.08 V at a current density of

0.1 mA cm^{-2}[246]. The polarization voltage of pure PVDF electrolyte is higher than 0.2 V, showing uniform lithium deposition. The assembled Li|PL$(Ga_{0.1}Ta_{0.3})_{25}$|LFP battery showed a capacity retention rate of 91.1% after 100 cycles at 0.2 C.

The incorporation of fillers can mitigate the formation of lithium dendrites and decrease the incidence of side reactions. For example, the DMF solvent in PVDF transfers Li ions by solvating with Li ions to form $[Li(DMF)_x]^+$ complexes. However, the side reaction between DMF and lithium metal leads to low coulomb efficiency and capacity attenuation during the battery cycle. The incorporation of fillers can absorb the solvent within the polymer, facilitate uniform distribution, and establish an inorganic layer at the lithium anode to mitigate the incidence of side reactions[247]. Li *et al.* added LATP to the PVDF electrolyte to prepare the electrolyte[248]. The assembled Li|PVDF/LATP/LiTFSI|LFP battery had an initial discharge-specific capacity of 150 mAh g^{-1}. After 50 cycles, the specific capacity remains at 130 mAh g^{-1}, in contrast to the electrolyte devoid of LATP, which exhibits a specific capacity of 54 mAh g^{-1} on the 50th cycle; the battery performance has markedly enhanced.

Increase battery energy density

The primary approach to enhance the energy density of a battery is to elevate its charging cut-off voltage, so it is necessary to match the high-voltage electrode material. However, the low electrochemical stability window limits the matching of PSEs to the high voltage electrode, and the filler can improve the electrochemical window of the electrolyte and reduce its resistance to oxidation and decomposition at high potential. Enhancing the intermolecular interaction forces in CSSEs is a common way to improve the electrochemical window[249].

Wang *et al.* added SiO_2 to poly(vinyl ethylene carbonate) (PVEC) to prepare the electrolyte[250]. Hydrogen bonding between the -OH on the surface of SiO_2 and the C=O group on PVEC enhanced the antioxidant capacity of the electrolyte. The electrochemical window of PVEC was elevated from 4.5 to 5.0 V. The capacity retention rate of the built Li|PVEC/SiO_2|$LiCo_2$ battery remained at 94% after 200 cycles at 25 °C. The capacity retention rate of the built battery lacking SiO_2 electrolyte was merely 20% after 50 cycles. Mu *et al.* filled directional $Li_{6.4}La_3Zr_2Al_{0.2}O_{12}$ (LLZAO) nanofibers into PEGDA, and the prepared electrolyte not only showed good lithium dendrite inhibition ability but also formed a cathode-electrolyte interface layer rich in LiF on the NCM811 cathode[251]. It significantly diminishes the frequency of side reactions at elevated pressure circumstances. The assembled Li|PEGDA/LLZAO|NCM811 battery exhibits a high specific capacity of 189.6 mAh g^{-1} at 0.1 C.

CONCLUSION AND OUTLOOK

Conclusion

This review introduces the key parameters of CSSEs and reviews the construction of lithium-ion transport channels. Furthermore, it discusses the effects of different types of fillers on the CSSEs. In this review, a comprehensive analysis of the critical roles played by fillers in CSSEs include: (1) Fillers reduce crystallinity; (2) The interface between filler and polymer creates a lithium-ion channel. Additionally, active fillers that conduct Li ions can offer supplementary transport channels for Li ions; and (3) The size and morphology of fillers exert varying degrees of influence on the performance of CSSEs. The fillers with a higher specific surface area can offer increased lithium-ion transport channels at the filler/polymer interface, which is crucial for enhancing the ionic conductivity of CSSEs. The 3D frame structures prepared using active fillers establish a continuous network for lithium-ion conduction, thus holding promise for overcoming the bottleneck in CSSEs ionic conductivity while achieving enhanced mechanical strength. In addition, the preparation methods and characterization techniques of fillers and CSSEs were also discussed. This review

focuses on the intimate interplay between filler materials and the mechanism of lithium-ion transport channels, encompassing the functional role of fillers and their underlying action principles. By synthesizing the latest research findings, an in-depth analysis is conducted to elucidate the structure-activity relationship between fillers and lithium-ion channels, thereby providing a robust foundation for the selection and dosage of fillers while ensuring optimal performance of CSSEs.

Outlook

Although this review summarizes many research works on CSSEs, for now, CSSEs research still has a high potential for exploitation. To achieve early and widespread use of CSSEs, further efforts should be made about the following challenges.

Advanced computer simulation techniques to further understand lithium-ion transport mechanisms

Further understanding of lithium-ion transport mechanisms. Following the introduction of the solid-state ionic conductor, numerous investigations have been undertaken to elucidate the lithium-ion transport process in diverse SSEs. However, the CSSE system is huge, especially the ionic conduction behaviors at the interfaces between fillers/polymers and CSSEs/electrodes are even more complex, so it is necessary to conduct more in-depth studies on the ionic conduction mechanisms. For example, advanced simulation techniques, such as molecular dynamics simulation (MD) and density flood theory calculations (DFT), are used to probe the thermodynamic and kinetic behaviors during lithium-ion migration, and combined with experiments to jointly study Li ion conduction in CSSEs.

Achieve higher ionic conductivity

The ionic conductivity of CSSEs surpasses that of conventional PSEs; there is still a big gap between CSSEs and liquid electrolytes currently used, which hinders the application of ASSLMBs with high energy density. It is anticipated that the existing limitation of ion conductivity in CSSEs might be surpassed by meticulously modifying the properties of the filler and the dispersion method inside the polymer matrix.

Standard evaluation of CSSEs' mechanical strength

A standardized method for evaluating the mechanical performance of CSSEs is essential to characterize their mechanical strength. While most current studies assess the mechanical properties of CSSEs based on tensile strength, variations in test conditions (such as tensile speed) pose challenges in comparing findings across different studies. It is imperative to quantify parameters such as elastic modulus and shear modulus to effectively evaluate CSSEs under diverse application conditions.

CSSEs for both thickness and mechanical properties

Currently, the thickness of most CSSEs still exceeds that of commercial polyolefin diaphragms. The development of ultra-thin CSSEs with enhanced strength and flexibility contributes to the improvement of battery energy density.

Selection of new fillers and polymer matrix

Currently, the polymer matrix of CSSEs is still dominated by PEO, PVDF, and PAN. Still, the problems of these materials need to be solved fundamentally: the high crystallinity of PEO at room temperature, the residual solvent in PVDF, and the instability between PAN and lithium metal still limit the broad application of CSSEs. Although fillers can solve the above problems to a certain extent, the research on fillers is still exploratory. In the future, more research should be carried out on the polymer chain structure, such as adopting the method of blocking or grafting to design functional groups in polymers and developing new types of fillers with special functions to realize the excellent performance of CSSEs.

Improve electrode/electrolyte interface issues

With the advancement of research on the design and synthesis of CSSEs, the electrode/electrolyte interface problem remains a significant challenge. Improving the adhesion and mechanical strength of CSSEs can be an excellent response to the issues of interfacial contact and lithium dendrite growth. Developing new structural design and process methods for CSSEs is a very promising strategy, such as *in situ* construction of a lithium-ion conductive layer on the electrolyte film surface to reduce the interfacial resistance, which makes CSSEs promising to match with electrodes with higher energy densities and high voltages.

Large-scale commercialization production line of CSSEs

Mature CSSE films suitable for industrialization are critical in energy storage. So far, many companies have started ASSLMB projects. For instance, Toyota in Japan has researched the energy density of a 400-500 Wh kg^{-1} sulfide electrolyte. However, there is still limited research on CSSEs. To promote the use of ASSLMBs, companies need to focus on enhancing the performance of CSSEs and developing cost-effective and efficient industrial production processes. Although solid-state batteries eliminate the need for liquid injection, they currently lack sufficient durability to address challenges such as battery winding. Therefore, specialized synthesis equipment is necessary to improve the mechanical properties and pore characteristics of SSEs. It is expected that dedicated production lines for SSE films will be established in the future.

DECLARATIONS

Acknowledgments

We acknowledge Wenyi Lu, Xiangrui Deng, Weizhuo Liu, and Pinyan Chen who contributed to the article.

Authors' contributions

Made substantial contributions to conception and design of the study and performed data collection and visualization: Wang Z, Yang H, Li S

Performed data acquisition and provided administrative, technical, and material support: Tong H, Xu W, Zhao Y, Li L

Availability of data and materials

The data are made available upon request to authors.

Financial support and sponsorship

This work was supported by the Harbin Manufacturing Science and Technology Innovation Talent Project [2022CXRCCG007], Heilongjiang Province Ecological Environment Protection Research Project [HST2022DQ007], and the National Natural Science Foundation of China [21706043].

Conflicts of interest

All authors declared that there are no conflicts of interest.

Ethical approval and consent to participate

Not applicable.

Consent for publication

Not applicable.

REFERENCES

1. Deng Y, Hussain A, Raza W, Cai X, Liu D, Shen J. Review on current development of polybenzimidazole membrane for lithium battery. *J Energy Chem* 2024;91:579-608. DOI
2. Huang J, Cheng L, Zhang Z, et al. High-performance all-solid-state lithium metal batteries enabled by ionic covalent organic framework composites. *Adv Energy Mater* 2024;14:2400762. DOI
3. Ye M, Chen J, Deng H, et al. *In-situ* electrochemical passivation for constructing high-voltage PEO-based solid-state lithium battery. *Chem Eng J* 2024;488:151108. DOI
4. Zhang X, Xu P, Duan J, et al. A dicarbonate solvent electrolyte for high performance 5 V-Class lithium-based batteries. *Nat Commun* 2024;15:536. DOI PubMed PMC
5. Li X, Kim JT, Luo J, et al. Structural regulation of halide superionic conductors for all-solid-state lithium batteries. *Nat Commun* 2024;15:53. DOI PubMed PMC
6. Cheng H, Yan C, Chang L, Dirican M, Orenstein R, Zhang X. Garnet-type composite polymer electrolyte for room-temperature all-solid-state Li-S battery. *ACS Appl Energy Mater* 2024;7:3071-81. DOI
7. Wei Y, Li Z, Chen Z, et al. Polymeric electronic shielding layer enabling superior dendrite suppression for all-solid-state lithium batteries. *Acs Nano* 2024;18:5965-80. DOI
8. Mu Y, Chen Y, Wu B, Zhang Q, Lin M, Zeng L. Dual vertically aligned electrode-inspired high-capacity lithium batteries. *Adv Sci* 2022;9:2203321. DOI PubMed PMC
9. Dong S, Sheng L, Wang L, et al. Challenges and prospects of all-solid-state electrodes for solid-state lithium batteries. *Adv Funct Mater* 2023;33:2304371. DOI
10. Zhang Y, Wang J, Xue Z. Electrode protection and electrolyte optimization via surface modification strategy for high-performance lithium batteries. *Adv Funct Mater* 2024;34:2311925. DOI
11. Zhang T, He W, Zhang W, et al. Designing composite solid-state electrolytes for high performance lithium ion or lithium metal batteries. *Chem Sci* 2020;11:8686-707. DOI
12. Castillo J, Qiao L, Santiago A, et al. Perspective of polymer-based solid-state Li-S batteries. *Energy Mater* 2022;2:200003. DOI
13. Yang B, Li T, Pan Y, et al. Design strategy towards flame-retardant gel polymer electrolytes for safe lithium metal batteries. *Energy Mater* 2024;4:400061. DOI
14. Orenstein R, Li Z, Dirican M, et al. A comparatively low cost, easy-to-fabricate, and environmentally friendly PVDF/garnet composite solid electrolyte for use in lithium metal cells paired with lithium iron phosphate and silicon. *ACS Appl Mater Interfaces* 2024;16:33428-38. DOI
15. Cheng H, Yan C, Orenstein R, et al. Polyacrylonitrile nanofiber-reinforced flexible single-ion conducting polymer electrolyte for high-performance, room-temperature all-solid-state Li-metal batteries. *Adv Fiber Mater* 2022;4:532-46. DOI
16. Zhang T, Shao Y, Zhang X, et al. Fast lithium ionic conductivity in complex hydride-sulfide electrolytes by double anions substitution. *Small Methods* 2021;5:2100609. DOI
17. Xu L, Li J, Shuai H, et al. Recent advances of composite electrolytes for solid-state Li batteries. *J Energy Chem* 2022;67:524-48. DOI
18. Liu S, Liu W, Ba D, et al. Filler-integrated composite polymer electrolyte for solid-state lithium batteries. *Adv Mater* 2023;35:2110423. DOI
19. Kim S, Lee H, Park J, Ku M, Kim M, Kim YB. Lithium-preserved sintering method for perovskite-based solid electrolyte thin films via flash light sintering for all-solid-state lithium-ion batteries. *J Mater Chem A* 2023;11:21586-94. DOI
20. Xue S, Chen S, Fu Y, et al. Revealing the role of active fillers in Li-ion conduction of composite solid electrolytes. *Small* 2023;19:2305326. DOI
21. Cui P, Sun C, Wei W. Polyurethane/$Li_{10}GeP_2S_{12}$ composite electrolyte with high ions transfer number and ions capture for all-solid-state lithium batteries. *Energy Mater* 2023;3:300017. DOI
22. Wang X, Jiang W, Zhu X, et al. A dynamically stable sulfide electrolyte architecture for high-performance all-solid-state lithium metal batteries. *Small* 2024;20:2306763. DOI
23. Cai M, Jin J, Xiu T, Song Z, Badding ME, Wen Z. *In situ* constructed lithium-salt lithiophilic layer inducing bi-functional interphase for stable LLZO/Li interface. *Energy Storage Mater* 2022;47:61-9. DOI
24. Luo L, Zheng F, Gao H, et al. Tuning the electron transport behavior at Li/LATP interface for enhanced cyclability of solid-state Li batteries. *Nano Res* 2023;16:1634-41. DOI
25. Gu T, Chen L, Huang Y, et al. Engineering ferroelectric interlayer between $Li_{1.3}Al0_3Ti_{1.7}(PO_4)_3$ and lithium metal for stable solid-state batteries operating at room temperature. *Energy Environ Mater* 2023;6:e12531. DOI
26. Wang L, Wang L, Shi Q, et al. In-situ constructed SnO_2 gradient buffer layer as a tight and robust interphase toward Li metal anodes in LATP solid-state batteries. *J Energy Chem* 2023;80:89-98. DOI
27. Li Z, Fu J, Zhou X, et al. Ionic conduction in polymer-based solid electrolytes. *Adv Sci* 2023;10:2201718. DOI PubMed PMC
28. Zhang N, Wu S, Zheng H, Li G, Liu H, Duan H. Recent progress of multilayer polymer electrolytes for lithium batteries. *Energy Mater* 2023;3:300009. DOI
29. Zhou D, Shanmukaraj D, Tkacheva A, Armand M, Wang G. Polymer electrolytes for lithium-based batteries: advances and prospects. *Chem* 2019;5:2326-52. DOI
30. Sun Y, Wang J, Fu D, et al. Flexible composite solid electrolyte with an active inorganic filler. *ACS Sustain Chem Eng* 2021;9:2237-

45. DOI
31. Bresser D, Hosoi K, Howell D, et al. Perspectives of automotive battery R&D in China, Germany, Japan, and the USA. *J Power Sources* 2018;382:176-68. DOI
32. Li T, Panda PK, Hsieh CT, Gandomi YA, Yang PC. Lithium iron phosphate cathode supported solid lithium batteries with dual composite solid electrolytes enabling high energy density and stable cyclability. *J Energy Storage* 2024;81:110444. DOI
33. Park S, Chaudhary R, Han SA, et al. Ionic conductivity and mechanical properties of the solid electrolyte interphase in lithium metal batteries. *Energy Mater* 2023;3:300005. DOI
34. Wang Y, Wang Q, Zhang D, et al. Enabling stable interface by constructing asymmetric organic-inorganic bi-functional composite electrolyte of high-voltage lithium metal batteries. *J Energy Storage* 2024;91:112099. DOI
35. Wei L, Xu X, Xi K, et al. Ultralong cycling and interfacial regulation of bilayer heterogeneous composite solid-state electrolytes in lithium metal batteries. *ACS Appl Mater Interfaces* 2024;16:33578-89. DOI
36. Liu Y, He P, Zhou H. Rechargeable solid-state Li-air and Li-S batteries: materials, construction, and challenges. *Adv Energy Mater* 2018;8:1701402. DOI
37. Zhou J, Wang X, Fu J, et al. A 3D cross-linked metal-organic framework (MOF)-derived polymer electrolyte for dendrite-free solid-state lithium-ion batteries. *Small* 2024;20:2309317. DOI
38. Zhou S, Han Z, Wang X, et al. Low-cost and high-safety montmorillonite-based solid electrolyte for lithium metal batteries. *Appl Clay Sci* 2024;251:107329. DOI
39. Chang Z, Qiao Y, Yang H, et al. Sustainable lithium-metal battery achieved by a safe electrolyte based on recyclable and low-cost molecular sieve. *Angew Chem Int Ed* 2021;60:15572-81. DOI
40. Lin D, Liu W, Liu Y, et al. High ionic conductivity of composite solid polymer electrolyte via in situ synthesis of monodispersed SiO_2 nanospheres in poly(ethylene oxide). *Nano Lett* 2016;16:459-65. DOI
41. Liu W, Lin D, Sun J, Zhou G, Cui Y. Improved lithium ionic conductivity in composite polymer electrolytes with oxide-ion conducting nanowires. *ACS Nano* 2016;10:11407-13. DOI
42. Chen L, Li W, Fan LZ, Nan CW, Zhang Q. Intercalated electrolyte with high transference number for dendrite-free solid-state lithium batteries. *Adv Funct Mater* 2019;29:1901047. DOI
43. Bae J, Li Y, Zhang J, et al. A 3D Nanostructured hydrogel-framework-derived high-performance composite polymer lithium-ion electrolyte. *Angew Chem Int Ed* 2018;57:2096-100. DOI
44. Zhu M, Wu J, Zhong WH, Lan J, Sui G, Yang X. A Biobased Composite gel polymer electrolyte with functions of lithium dendrites suppressing and manganese ions trapping. *Adv Energy Mater* 2018;8:1702561. DOI
45. Xu H, Chien PH, Shi J, et al. High-performance all-solid-state batteries enabled by salt bonding to perovskite in poly(ethylene oxide). *P Natl Aca Sci USA* 2019;116:11815-21. DOI PubMed PMC
46. Bae J, Li Y, Zhao F, Zhou X, Ding Y, Yu G. Designing 3D nanostructured garnet frameworks for enhancing ionic conductivity and flexibility in composite polymer electrolytes for lithium batteries. *Energy Storage Mater* 2018;15:46-52. DOI
47. Zhou Q, Ma J, Dong S, Li X, Cui G. Intermolecular chemistry in solid polymer electrolytes for high-energy-density lithium batteries. *Adv Mater* 2019;31:1902029. DOI
48. Shen Z, Cheng Y, Sun S, Ke X, Liu L, Shi Z. The critical role of inorganic nanofillers in solid polymer composite electrolyte for Li^+ transportation. *Carbon Energy* 2021;3:482-508. DOI
49. Maitra A, Heuer A. Cation transport in polymer electrolytes: a microscopic approach. *Phys Rev Lett* 2007;98:227802. DOI PubMed
50. Zhou S, Zhong S, Dong Y, et al. Composition and structure design of poly(vinylidene fluoride)-based solid polymer electrolytes for lithium batteries. *Adv Funct Mater* 2023;33:2214432. DOI
51. Zhao Y, Li L, Zhou D, et al. Opening and constructing stable lithium-ion channels within polymer electrolytes. *Angew Chem Int Ed* 2024;63:202404728. DOI
52. Zhang Q, Liu K, Ding F, Liu X. Recent advances in solid polymer electrolytes for lithium batteries. *Nano Res* 2017;10:4139-74. DOI
53. Lin Q, Kundu D, Skyllas-Kazacos M, et al. Perspective on lewis acid-base interactions in emerging batteries. *Adv Mater* 2024;36:2406151. DOI
54. Rajendran S, Uma T. Effect of ceramic oxide on PVC-PMMA hybrid polymer electrolytes. *Ionics* 2000;6:288-93. DOI
55. Ma C, Dai K, Hou H, et al. High ion-conducting solid-state composite electrolytes with carbon quantum dot nanofillers. *Adv Sci* 2018;5:1700996. DOI PubMed PMC
56. Zhang J, Zhao N, Zhang M, et al. Flexible and ion-conducting membrane electrolytes for solid-state lithium batteries: dispersion of garnet nanoparticles in insulating polyethylene oxide. *Nano Energy* 2016;28:447-54. DOI
57. Zhang B, Tan R, Yang L, et al. Mechanisms and properties of ion-transport in inorganic solid electrolytes. *Energy Storage Mater* 2018;10:139-59. DOI
58. Park M, Zhang X, Chung M, Less GB, Sastry AM. A review of conduction phenomena in Li-ion batteries. *J Power Sources* 2010;195:7904-29. DOI
59. Islam MS, Driscoll DJ, Fisher CAJ, Slater PR. Atomic-scale investigation of defects, dopants, and lithium transport in the $LiFePO_4$ olivine-type battery material. *Chem Mater* 2005;17:5085-92. DOI
60. Chroneos A, Yildiz B, Tarancón A, Parfitt D, Kilner JA. Oxygen diffusion in solid oxidefuel cell cathode and electrolyte materials: mechanistic insights from atomistic simulations. *Energy Environ Sci* 2011;4:2774-89. DOI
61. Li Z, Huang HM, Zhu JK, et al. Ionic conduction in composite polymer electrolytes: case of PEO:Ga-LLZO composites. *ACS Appl*

Mater Interfaces 2019;11:784-91. DOI

62. Mohapatra SR, Thakur AK, Choudhary RNP. Effect of nanoscopic confinement on improvement in ion conduction and stability properties of an intercalated polymer nanocomposite electrolyte for energy storage applications. *J Power Sources* 2009;191:601-13. DOI
63. Zheng J, Tang M, Hu YY. Lithium ion pathway within $Li_7La_3Zr_2O_{12}$-polyethylene oxide composite electrolytes. *Angew Chem Int Ed* 2016;55:12538-42. DOI
64. Yi E, Wang W, Kieffer J, Laine RM. Flame made nanoparticles permit processing of dense, flexible, Li^+ conducting ceramic electrolyte thin films of cubic-$Li_7La_3Zr_2O_{12}$ (c-LLZO). *J Mater Chem A* 2016;4:12947-54. DOI
65. Zheng Y, Yao Y, Ou J, et al. A review of composite solid-state electrolytes for lithium batteries: fundamentals, key materials and advanced structures. *Chem Soc Rev* 2020;49:8790-839. DOI
66. Chen L, Li Y, Li SP, Fan LZ, Nan CW, Goodenough JB. PEO/garnet composite electrolytes for solid-state lithium batteries: from "ceramic-in-polymer" to "polymer-in-ceramic". *Nano Energy* 2018;46:176-84. DOI
67. Quartarone E, Mustarelli P. Electrolytes for solid-state lithium rechargeable batteries: recent advances and perspectives. *Chem Soc Rev* 2011;40:2525-40. DOI PubMed
68. Agrawal RC, Pandey GP. Solid polymer electrolytes: materials designing and all-solid-state battery applications: an overview. *J Phys D Appl Phys* 2008;41:223001. DOI
69. Goodenough JB. Oxide-ion electrolytes. *Annu Rev Mater Res* 2003;33:91-128. DOI
70. Dirican M, Yan C, Zhu P, Zhang X. Composite solid electrolytes for all-solid-state lithium batteries. *Mater Sci Eng R Rep* 2019;136:27-46. DOI
71. Diederichsen KM, Mcshane EJ, Mccloskey BD. Promising routes to a high Li^+ transference number electrolyte for lithium ion batteries. *Acs Energy Lett* 2017;2:2563-75. DOI
72. Nag A, Ali MA, Singh A, Vedarajan R, Matsumi N, Kaneko T. N-Boronated polybenzimidazole for composite electrolyte design of highly ion conducting pseudo solid-state ion gel electrolytes with a high Li-transference number. *J Mater Chem A* 2019;7:4459-68. DOI
73. Mindemark J, Lacey MJ, Bowden T, Brandell D. Beyond PEO-alternative host materials for Li^+-conducting solid polymer electrolytes. *Prog Polym Sci* 2018;81:114-43. DOI
74. Jia M, Khurram Tufail M, Guo X. Insight into the key factors in high Li^+ transference number composite electrolytes for solid lithium batteries. *ChemSusChem* 2022;16:e202201801. DOI
75. Wang GX, Yang L, Wang JZ, Liu HK, Dou SX. Enhancement of ionic conductivity of PEO based polymer electrolyte by the addition of nanosize ceramic powders. *J Nanosci Nanotechno* 2005;5:1135-40. PubMed
76. Shin JH, Kim KW, Ahn HJ, Ahn JH. Electrochemical properties and interfacial stability of $(PEO)_{10}LiCF_3SO_3$-Ti_nO_{2n-1} composite polymer electrolytes for lithium/sulfur battery. *Mater Sci Eng* 2002;95:148-56. DOI
77. Tamilselvi P, Hema M, Asath Bahadur S. Investigation of nanocomposite polymer electrolytes for lithium ion batteries. *Polym Sci Ser A* 2018;60:102-9. DOI
78. Lu G, Wei H, Shen C, et al. Bifunctional MOF doped PEO composite electrolyte for long-life cycle solid lithium ion battery. *ACS Appl Mater Interfaces* 2022;14:45476-83. DOI
79. Ren D, Tang X, Wang Q, Du H, Ding L. Aluminum-lithium alloy fillers enhancing the room temperature performances of polymer electrolytes for all-solid-state lithium batteries. *ACS Omega* 2024;9:35920-8. DOI PubMed PMC
80. Masoud EM, El-bellihi AA, Bayoumy WA, Mousa MA. Effect of $LiAlO_2$ nanoparticle filler concentration on the electrical properties of PEO-$LiClO_4$ composite. *Mater Res Bull* 2013;48:1148-54. DOI
81. Aravindan V, Vickraman P. Effects of TiO_2 and ZrO_2 nanofillers in LiBOB based PVDF/PVC composite polymer electrolytes (CPE). *J Phys D Appl Phys* 2007;40:6754. DOI
82. Zhang Y, Wang X, Feng W, et al. Effects of the shapes of $BaTiO_3$ nanofillers on PEO-based electrolytes for all-solid-state lithium-ion batteries. *Ionics* 2018;25:1471-80. DOI
83. Xi J, Qiu X, Zhu W, Tang X. Enhanced electrochemical properties of poly(ethylene oxide)-based composite polymer electrolyte with ordered mesoporous materials for lithium polymer battery. *Micropor Mesopor Mater* 2006;88:1-7. DOI
84. Zhang Y, Zhao Y, Gosselink D, Chen P. Synthesis of poly(ethylene-oxide)/nanoclay solid polymer electrolyte for all solid-state lithium/sulfur battery. *Ionics* 2014;21:381-5. DOI
85. Ma Y, Li LB, Gao GX, Yang XY, You Y. Effect of montmorillonite on the ionic conductivity and electrochemical properties of a composite solid polymer electrolyte based on polyvinylidenedifluoride/polyvinyl alcohol matrix for lithium ion batteries. *Electrochim Acta* 2015;187:535-42. DOI
86. Milian Pila CR, Cappe EP, Mohallem NDS, et al. Effect of the LLTO nanoparticles on the conducting properties of PEO-based solid electrolyte. *Solid State Sci* 2019;88:41-7. DOI
87. Zhou D, Zhang M, Sun F, et al. Performance and behavior of LLZO-based composite polymer electrolyte for lithium metal electrode with high capacity utilization. *Nano Energy* 2020;77:105196. DOI
88. Yu X, Liu Y, Goodenough JB, Manthiram A. Rationally designed PEGDA-LLZTO composite electrolyte for solid-state lithium batteries. *ACS Appl Mater Interfaces* 2021;13:30703-11. DOI
89. Li X, Wang D, Wang H, Yan H, Gong Z, Yang Y. Poly(ethylene oxide)-$Li_{10}SnP_2S_{12}$ composite polymer electrolyte enables high-performance all-solid-state lithium sulfur battery. *ACS Appl Mater Interfaces* 2019;11:22745-53. DOI

90. Li D, Chen L, Wang T, Fan LZ. 3D fiber-network-reinforced bicontinuous composite solid electrolyte for dendrite-free lithium metal batteries. *ACS Appl Mater Interfaces* 2018;10:7069-78. DOI
91. Xu A, Wang R, Yao M, et al. Electrochemical properties of an Sn-doped LATP ceramic electrolyte and its derived sandwich-structured composite solid electrolyte. *Nanomaterials* 2022;12:2082. DOI PubMed PMC
92. Zhu L, Zhu P, Yao S, Shen X, Tu F. High-performance solid PEO/PPC/LLTO-nanowires polymer composite electrolyte for solid-state lithium battery. *Int J Energy Res* 2019;43:4854-66. DOI
93. Xu H, Huang S, Qian J, et al. Safe solid-state PEO/TPU/LLZO nano network polymer composite gel electrolyte for solid state lithium batteries. *Colloid Surface A* 2022;653:130040. DOI
94. Zhai H, Xu P, Ning M, Cheng Q, Mandal J, Yang Y. A flexible solid composite electrolyte with vertically aligned and connected ion-conducting nanoparticles for lithium batteries. *Nano Lett* 2017;17:3182-7. DOI
95. Fu KK, Gong Y, Dai J, et al. Flexible, solid-state, ion-conducting membrane with 3D garnet nanofiber networks for lithium batteries. *Proc Natl Acad Sci USA* 2016;113:7094-9. DOI
96. Chen R, Li Q, Yu X, Chen L, Li H. Approaching practically accessible solid-state batteries: stability issues related to solid electrolytes and interfaces. *Chem Rev* 2020;120:6820-77. DOI
97. Li Z, Xie HX, Zhang XY, Guo X. *In situ* thermally polymerized solid composite electrolytes with a broad electrochemical window for all-solid-state lithium metal batteries. *J Mater Chem A* 2020;8:3892-900. DOI
98. Zhu Y, He X, Mo Y. First principles study on electrochemical and chemical stability of solid electrolyte-electrode interfaces in all-solid-state Li-ion batteries. *J Mater Chem A* 2016;4:3253-66. DOI
99. Li B, Wang C, Yu R, et al. Recent progress on metal-organic framework/polymer composite electrolytes for solid-state lithium metal batteries: ion transport regulation and interface engineering. *Energy Environ Sci* 2024;17:1854-84. DOI
100. Zhao W, Yi J, He P, Zhou H. Solid-state electrolytes for lithium-ion batteries: fundamentals, challenges and perspectives. *Electrochem Energy Rev* 2019;2:574-605. DOI
101. Chu Y, Shen Y, Guo F, et al. Advanced characterizations of solid electrolyte interphases in lithium-ion batteries. *Electrochem Energy Rev* 2020;3:187-219. DOI
102. Zhang Q, Yue B, Shao C, et al. Suppression of lithium dendrites in all-solid-state lithium batteries by using a Janus-structured composite solid electrolyte. *Chem Eng J* 2022;443:136479. DOI
103. Dong D, Zhou B, Sun Y, et al. Polymer electrolyte glue: a universal interfacial modification strategy for all-solid-state Li batteries. *Nano Lett* 2019;19:2343-9. DOI
104. Su H, Li J, Zhong Y, et al. A scalable Li-Al-Cl stratified structure for stable all-solid-state lithium metal batteries. *Nat Commun* 2024;15:4202. DOI PubMed PMC
105. Jia L, Zhu J, Zhang X, Guo B, Du Y, Zhuang X. Li-solid electrolyte interfaces/interphases in all-solid-state Li batteries. *Electrochem Energy Rev* 2024;7:12. DOI
106. Zhang J, Li S, Wang X, et al. Construction of stable Li_2O-rich solid electrolyte interphase for practical PEO-based Li-metal batteries. *Adv Energy Mater* 2023;14:2302587. DOI
107. Famprikis T, Canepa P, Dawson JA, Islam MS, Masquelier C. Fundamentals of inorganic solid-state electrolytes for batteries. *Nat Mater* 2019;18:1278-91. DOI PubMed
108. Yu S, Schmidt RD, Garcia-Mendez R, et al. Elastic properties of the solid electrolyte $Li_7La_3Zr_2O_{12}$ (LLZO). *Chem Mater* 2016;28:197-206. DOI
109. Du A, Lu H, Liu S, et al. Breaking the trade-off between ionic conductivity and mechanical strength in solid polymer electrolytes for high-performance solid lithium batteries. *Adv Energy Mater* 2024;14:2400808. DOI
110. Weston JE, Steele BCH. Effects of inert fillers on the mechanical and electrochemical properties of lithium salt-poly(ethylene oxide) polymer electrolytes. *Solid State Ion* 1982;7:75-9. DOI
111. Chen G, Lu J, Li L, Chen L, Jiang X. Microstructure control and properties of β"-Al_2O_3 solid electrolyte. *J Alloy Compd* 2016;673:295-301. DOI
112. Zhao R, Wu Y, Liang Z, et al. Metal-organic frameworks for solid-state electrolytes. *Energy Environ Sci* 2020;13:2386-403. DOI
113. Peta G, Bublil S, Alon-yehezkel H, et al. Toward high performance all solid-state Na batteries: investigation of electrolytes comprising $NaPF_6$, Poly(ethylene oxide) and TiO_2. *J Electrochem Soc* 2021;168:110553. DOI
114. Pan J, Zhao P, Yao H, Hu L, Fan HJ. Inert filler selection strategies in Li-ion gel polymer electrolytes. *ACS Appl Mater Interfaces* 2024;16:48706-12. DOI
115. Wang XL, Mei A, Li M, Lin YH, Nan CW. Polymer composite electrolytes containing ionically active mesoporous SiO_2 particles. *J Appl Phys* 2007;102:054907. DOI
116. Wang C, Yang T, Zhang W, et al. Hydrogen bonding enhanced SiO_2/PEO composite electrolytes for solid-state lithium batteries. *J Mater Chem A* 2022;10:3400-8. DOI
117. Tang S, Lan Q, Xu L, et al. A novel cross-linked nanocomposite solid-state electrolyte with super flexibility and performance for lithium metal battery. *Nano Energy* 2020;71:104600. DOI
118. Zhang Z, Zhang S, Geng S, Zhou S, Hu Z, Luo J. Agglomeration-free composite solid electrolyte and enhanced cathode-electrolyte interphase kinetics for all-solid-state lithium metal batteries. *Energy Storage Mater* 2022;51:19-28. DOI
119. Zhan H, Wu M, Wang R, et al. Excellent performances of composite polymer electrolytes with porous vinyl-functionalized SiO_2 nanoparticles for lithium metal batteries. *Polymers* 2021;13:2468. DOI PubMed PMC

120. Bao W, Zhao L, Zhao H, et al. Vapor phase infiltration of ZnO quantum dots for all-solid-state PEO-based lithium batteries. *Energy Storage Mater* 2021;43:258-65. DOI
121. Xia S, Zhao Y, Yan J, Yu J, Ding B. Dynamic regulation of lithium dendrite growth with electromechanical coupling effect of soft $BaTiO_3$ ceramic nanofiber films. *ACS Nano* 2021;15:3161-70. DOI
122. Acosta M, Novak N, Rojas V, et al. $BaTiO_3$-based piezoelectrics: fundamentals, current status, and perspectives. *Appl Phys Rev* 2017;4:041305. DOI
123. Singh PK, Chandra A. Role of the dielectric constant of ferroelectric ceramic in enhancing the ionic conductivity of a polymer electrolyte composite. *J Phys D Appl Phys* 2003;36:L93. DOI
124. Mazurenko I, Etienne M, Francius G, Vakulko I, Walcarius A. Macroporous carbon nanotube-carbon composite electrodes. *Carbon* 2016;109:106-16. DOI
125. Zhang E, Wang J, Wang B, Yu X, Yang H, Lu B. Unzipped carbon nanotubes for aluminum battery. *Energy Storage Mater* 2019;23:72-8. DOI
126. Delgado-Rosero MI, Jurado-Meneses NM, Uribe-Kaffure R. Composite polymer electrolytes based on $(PEO)_4CF_3COOLi$ and multi-walled carbon nanotube (MWCNT). *Polymers* 2023;15:49. DOI PubMed PMC
127. Tang C, Hackenberg K, Fu Q, Ajayan PM, Ardebili H. High ion conducting polymer nanocomposite electrolytes using hybrid nanofillers. *Nano Lett* 2012;12:1152-6. DOI PubMed
128. Wang A, Xu H, Liu X, et al. High electrochemical performances of solid nano-composite star polymer electrolytes enhanced by different carbon nanomaterials. *Compos Sci Technol* 2017;152:68-75. DOI
129. Zhu Y, Zheng Y, Liu J, et al. Molecular coupling strategy achieving in situ synthesis of agglomeration-free solid composite electrolytes. *J Phys Chem Lett* 2024;15:733-43. DOI
130. Zhao Y, Li L, Shan Y, et al. In situ construction channels of lithium-ion fast transport and uniform deposition to ensure safe high-performance solid batteries. *Small* 2023;19:2301572. DOI
131. Jiang S, Lv T, Peng Y, Pang H. MOFs containing solid-state electrolytes for batteries. *Adv Sci* 2023;10:2206887. DOI PubMed PMC
132. Lei H, Tu J, Li S, et al. MOF-based quasi-solid-state electrolyte for long-life Al-Se battery. *J Energy Chem* 2023;86:237-45. DOI
133. Lu C, Wu Y, Rong Y, et al. Dual-functional application of a metal-organic framework in high-performance all-solid-state lithium metal batteries. *Chem Eng J* 2023;475:146152. DOI
134. Wang Z, Zhou H, Meng C, et al. Enhancing ion transport: function of ionic liquid decorated MOFs in polymer electrolytes for all-solid-state lithium batteries. *ACS Appl Energy Mater* 2020;3:4265-74. DOI
135. Miao Z, Zhang F, Zhao H, et al. Tailoring local electrolyte solvation structure via a mesoporous molecular sieve for dendrite-free zinc batteries. *Adv Funct Mater* 2022;32:2111635. DOI
136. Jiang YX, Chen ZF, Zhuang QC, et al. A novel composite microporous polymer electrolyte prepared with molecule sieves for Li-ion batteries. *J Power Sources* 2006;160:1320-8. DOI
137. Ding Z, Tang Q, Zhang Q, Yao P, Liu X, Wu J. A flexible solid polymer electrolyte enabled with lithiated zeolite for high performance lithium battery. *Nano Res* 2023;16:9443-52. DOI
138. Lu J, Li Y. Perovskite-type Li-ion solid electrolytes: a review. *J Mater Sci Mater Electron* 2021;32:9736-54. DOI
139. Lu J, Li Y, Ding Y. Structure and conductivity of $Li_{3/8}Sr_{7/16x}A_xZr_{1/4}$ $Nb_{3/4}O_3$ (A = Ca, Ba) Li-ion solid electrolytes. *JOM* 2020;72:3256-61. DOI
140. Mitsuishi K, Ohnishi T, Tanaka Y, et al. Nazca lines by La ordering in $La_{2/3-x}Li_{3x}TiO_3$ ion-conductive perovskite. *Appl Phys Lett* 2012;101:073903. DOI
141. Lu J, Li Y, Ding Y. Li-ion conductivity and electrochemical stability of A-site deficient perovskite-structured $Li_{3x-y}La_{1-x}Al_{1-y}Ti_yO_3$ electrolytes. *Mater Res Bull* 2020;133:111019. DOI
142. Hua C, Fang X, Wang Z, Chen L. Lithium storage in perovskite lithium lanthanum titanate. *Electrochem Commun* 2013;32:5-8. DOI
143. Lu J, Li Y, Ding Y. Structure, stability, and ionic conductivity of perovskite $Li_{2x-y}Sr_{1-x-y}La_yTiO_3$ solid electrolytes. *Ceram Int* 2020;46:7741-7. DOI
144. Yu K, Jin L, Li Y, Liu G, Wei X, Yan Y. Structure and conductivity of perovskite $Li_{0.355}La_{0.35}Sr_{0.3}Ti_{0.995}M_{0.005}O_3$ (M = Al, Co and In) ceramics. *Ceram Int* 2019;45:23941-7. DOI
145. Lee SJ, Bae JJ, Son JT. Structural and electrical effects of Y-doped $Li_{0.33}La_{0.56-x}Y_xTiO_3$ solid electrolytes on all-solid-state lithium ion batteries. *J Korean Phys Soc* 2019;74:73-7. DOI
146. Dixit M, Muralidharan N, Bisht A, et al. Tailoring of the anti-perovskite solid electrolytes at the grain-scale. *ACS Energy Lett* 2023;8:2356-64. DOI
147. Gao L, Zhang X, Zhu J, et al. Boosting lithium ion conductivity of antiperovskite solid electrolyte by potassium ions substitution for cation clusters. *Nat Commun* 2023;14:6807. DOI PubMed PMC
148. Yoshikawa K, Yamamoto T, Sugumar MK, Motoyama M, Iriyama Y. Room temperature operation and high cycle stability of an all-solid-state lithium battery fabricated by cold pressing using soft Li_2OHBr solid electrolyte. *Energy Fuels* 2021;35:12581-7. DOI
149. Lü X, Howard JW, Chen A, et al. Antiperovskite Li_3OCl superionic conductor films for solid-state Li-ion batteries. *Adv Sci* 2016;3:1500359. DOI PubMed PMC
150. Ou J, Tatagari V, Senevirathna I, et al. On the formation and properties of amorphous and crystalline $Li_{3-y}Ba_{y/2}OCl$ electrolytes. *J Power Sources* 2024;609:234685. DOI

151. Zhang Y, Meng Z, Wang Y. Sr doped amorphous LLTO as solid electrolyte material. *J Electrochem Soc* 2020;167:080516. DOI
152. Romero M, Faccio R, Vázquez S, Mombrú ÁW. Enhancement of lithium conductivity and evidence of lithium dissociation for LLTO-PMMA nanocomposite electrolyte. *Mater Lett* 2016;172:1-5. DOI
153. Xia W, Zhao Y, Zhao F, et al. Antiperovskite electrolytes for solid-state batteries. *Chem Rev* 2022;122:3763-819. DOI
154. Dawson JA, Attari TS, Chen H, Emge SP, Johnston KE, Islam MS. Elucidating lithium-ion and proton dynamics in anti-perovskite solid electrolytes. *Energy Environ Sci* 2018;11:2993-3002. DOI
155. Wang Y, Richards WD, Ong SP, et al. Design principles for solid-state lithium superionic conductors. *Nat Mater* 2015;14:1026-31. DOI
156. Ye Y, Deng Z, Gao L, et al. Lithium-rich anti-perovskite Li_2OHBr-based polymer electrolytes enabling an improved interfacial stability with a three-dimensional-structured lithium metal anode in all-solid-state batteries. *ACS Appl Mater Interfaces* 2021;13:28108-17. DOI
157. Wang C, Fu K, Kammampata SP, et al. Garnet-type solid-state electrolytes: materials, interfaces, and batteries. *Chem Rev* 2020;120:4257-300. DOI
158. Thangadurai V, Narayanan S, Pinzaru D. Garnet-type solid-state fast Li ion conductors for Li batteries: critical review. *Chem Soc Rev* 2014;43:4714-27. DOI PubMed
159. O'callaghan MP, Powell AS, Titman JJ, Chen GZ, Cussen EJ. Switching on fast lithium ion conductivity in Garnets: the structure and transport properties of $Li_{3+x}Nd_3Te_{2-x}Sb_xO_{12}$. *Chem Mater* 2008;20:2360-9. DOI
160. Xie H, Alonso JA, Li Y, Fernández-Díaz MT, Goodenough JB. Lithium distribution in aluminum-Free cubic $Li_7La_3Zr_2O_{12}$. *Chem Mater* 2011;23:3587-9. DOI
161. Li Y, Han JT, Wang CA, Xie H, Goodenough JB. Optimizing Li^+ conductivity in a garnet framework. *J Mater Chem* 2012;22:15357-61. DOI
162. Murugan R, Thangadurai V, Weppner W. Fast lithium ion conduction in garnet-type $Li_7La_3Zr_2O_{12}$. *Angew Chem Int Ed* 2007;46:7778-81. DOI
163. Kodgire P, Tripathi B, Chandra P. Review of garnet-based solid electrolytes for Li-ion batteries (LIBs). *J Electron Mater* 2024;53:2203-28. DOI
164. Kotobuki M, Koishi M. Preparation of $Li_7La_3Zr_2O_{12}$ solid electrolyte via a sol-gel method. *Ceram Int* 2014;40:5043-7. DOI
165. Wang C, Lin PP, Gong Y, Liu ZG, Lin TS, He P. Co-doping effects of Ba^{2+} and Ta^{5+} on the microstructure and ionic conductivity of garnet-type solid state electrolytes. *J Alloy Compd* 2021;854:157143. DOI
166. Wang D, Zhong G, Dolotko O, et al. The synergistic effects of Al and Te on the structure and Li^+-mobility of garnet-type solid electrolytes. *J Mater Chem A* 2014;2:20271-9. DOI
167. Dhivya L, Janani N, Palanivel B, Murugan R. Li^+ transport properties of W substituted $Li_7La_3Zr_2O_{12}$ cubic lithium Garnets. *Appl Phys Lett* 2013;3:089902. DOI
168. Luo Y, Li X, Zhang Y, Ge L, Chen H, Guo L. Electrochemical properties and structural stability of Ga- and Y- co-doping in $Li_7La_3Zr_2O_{12}$ ceramic electrolytes for lithium-ion batteries. *Electrochim Acta* 2019;294:217-25. DOI
169. Ramakumar S, Satyanarayana L, Manorama SV, Murugan R. Structure and Li^+ dynamics of Sb-doped $Li_7La_3Zr_2O_{12}$ fast lithium ion conductors. *Phys Chem Chem Phys* 2013;15:11327-38. DOI
170. Il'ina EA, Lyalin ED, Antonov BD, Pankratov AA, Vovkotrub EG. Sol-gel synthesis of Al- and Nb-co-doped $Li_7La_3Zr_2O_{12}$ solid electrolytes. *Ionics* 2020;26:3239-47. DOI
171. Bai L, Xue W, Xue Y, et al. Interfacial Ion-transport mechanism of $Li_7(Al_{0.1})La_3Zr_2O_{12}$ solid electrolyte modified by using a spark plasma sintering method. *ChemElectroChem* 2018;5:3918-25. DOI
172. Zhang Y, Deng J, Hu D, et al. Synergistic regulation of garnet-type Ta-doped $Li_7La_3Zr_2O_{12}$ solid electrolyte by Li^+ concentration and Li^+ transport channel size. *Electrochim Acta* 2019;296:823-9. DOI
173. Chen F, Yang D, Zha W, et al. Solid polymer electrolytes incorporating cubic $Li_7La_3Zr_2O_{12}$ for all-solid-state lithium rechargeable batteries. *Electrochim Acta* 2017;258:1106-14. DOI
174. Karthik K, Murugan R. Lithium garnet based free-standing solid polymer composite membrane for rechargeable lithium battery. *J Solid State Electrochem* 2018;22:2989-98. DOI
175. Nguyen HL, Luu VT, Nguyen MC, et al. Nb/Al co-doped $Li_7La_3Zr_2O_{12}$ composite solid electrolyte for high-performance all-solid-state batteries. *Adv Funct Mater* 2022;32:2207874. DOI
176. Lu Z, Peng L, Rong Y, et al. Enhanced electrochemical properties and optimized Li^+ transmission pathways of PEO/LLZTO-based composite electrolytes modified by supramolecular combination. *Energy Environ Mater* 2023;7:12498. DOI
177. Huo H, Chen Y, Luo J, Yang X, Guo X, Sun X. Rational design of hierarchical "ceramic-in-polymer" and "polymer-in-ceramic" electrolytes for dendrite-free solid-state batteries. *Adv Energy Mater* 2019;9:1804004. DOI
178. Danusso F, Tieghi G. Strength versus composition of rigid matrix particulate composites. *Polymer* 1986;27:1385-90. DOI
179. Yang K, Chen L, Ma J, He YB, Kang F. Progress and perspective of $Li_{1+x}Al_xTi_{2-x}(PO_4)_3$ ceramic electrolyte in lithium batteries. *InfoMat* 2021;3:1195-217. DOI
180. Boaretto N, Ghorbanzade P, Perez-Furundarena H, et al. Transport properties and local ions dynamics in LATP-based hybrid solid electrolytes. *Small* 2023;20:2305769. DOI
181. Arbi K, Bucheli W, Jiménez R, Sanz J. High lithium ion conducting solid electrolytes based on NASICON $Li_{1+x}Al_xM_{2-x}(PO_4)_3$ materials (M=Ti, Ge and $0 \leq x \leq 0.5$). *J Eur Ceram Soc* 2015;35:1477-84. DOI

182. Key B, Schroeder DJ, Ingram BJ, Vaughey JT. Solution-based synthesis and characterization of lithium-ion conducting phosphate ceramics for lithium metal batteries. *Chem Mater* 2012;24:287-93. DOI
183. Huang L, Wen Z, Wu M, Wu X, Liu Y, Wang X. Electrochemical properties of $Li_{1.4}Al_{0.4}Ti_{1.6}(PO_4)_3$ synthesized by a co-precipitation method. *J Power Sources* 2011;196:6943-6. DOI
184. Wu XM, Li XH, Zhang YH, Xu MF, He ZQ. Synthesis of $Li_{1.3}Al_{0.3}Ti_{1.7}(PO_4)_3$ by sol-gel technique. *Mater Lett* 2004;58:1227-30. DOI
185. Kosova NV, Devyatkina ET, Stepanov AP, Buzlukov AL. Lithium conductivity and lithium diffusion in NASICON-type $Li_{1+x}Ti_{2-x}Al_x(PO_4)_3$ (x = 0; 0.3) prepared by mechanical activation. *Ionics* 2008;14:303-11. DOI
186. Siller V, Morata A, Eroles MN, et al. High performance LATP thin film electrolytes for all-solid-state microbattery applications. *J Mater Chem A* 2021;9:17760-9. DOI
187. Kotobuki M, Koishi M. Preparation of $Li_{1.5}Al_{0.5}Ti_{1.5}(PO_4)_3$ solid electrolyte via a sol-gel route using various Al sources. *Ceram Int* 2013;39:4645-9. DOI
188. Berbano SS, Guo J, Guo H, Lanagan MT, Randall CA. Cold sintering process of $Li_{1.5}Al_{0.5}Ge_{1.5}(PO_4)_3$ solid electrolyte. *J Am Ceram Soc* 2017;100:2123-35. DOI
189. Kotobuki M, Yan B, Pan F, Lu L, Savilov S, Aldoshin S. Low temperature sintering of crystallized $Li_{1.5}Al_{0.5}Ge_{1.5}(PO_4)_3$ using hot-press technique. *Mater Today Pro* 2019;17:408-15. DOI
190. Liu Y, Chen J, Gao J. Preparation and chemical compatibility of lithium aluminum germanium phosphate solid electrolyte. *Solid State Ion* 2018;318:27-34. DOI
191. Kubanska A, Castro L, Tortet L, Schäf O, Dollé M, Bouchet R. Elaboration of controlled size $Li_{1.5}Al_{0.5}Ge_{1.5}(PO_4)_3$ crystallites from glass-ceramics. *Solid State Ion* 2014;266:44-50. DOI
192. Yan B, Kang L, Kotobuki M, He L, Liu B, Jiang K. Boron group element doping of $Li_{1.5}Al_{0.5}Ge_{1.5}(PO_4)_3$ based on microwave sintering. *J Solid State Electrochem* 2020;25:527-34. DOI
193. Liu Y, Li C, Li B, et al. Germanium thin film protected lithium aluminum germanium phosphate for solid-state Li batteries. *Adv Energy Mater* 2018;8:1702374. DOI
194. Yu J, Liu Q, Hu X, et al. Smart construction of multifunctional $Li_{1.5}Al_{0.5}Ge_{1.5}(PO_4)_3$|Li intermediate interfaces for solid-state batteries. *Energy Storage Mater* 2022;46:68-75. DOI
195. Sun Z, Liu L, Lu Y, et al. Preparation and ionic conduction of $Li_{1.5}Al_{0.5}Ge_{1.5}(PO_4)_3$ solid electrolyte using inorganic germanium as precursor. *J Eur Ceram Soc* 2019;39:402-8. DOI
196. Huang ZH, Li J, Li LX, et al. Boosting lithium-ion transport capability of LAGP/PPO composite solid electrolyte via component regulation from 'Ceramics-in-Polymer' to 'Polymer-in-Ceramics'. *Ceram Int* 2022;48:25949-57. DOI
197. Panda PK, Cho TS, Hsieh CT, Yang PC. Cobalt- and copper-doped NASICON-type LATP polymer composite electrolytes enabling lithium titania electrode for solid-state lithium batteries with high-rate capability and excellent cyclic performance. *J Energy Storage* 2024;95:112559. DOI
198. Lu X, Hai J, Zhang F, Li X, Li J. Preparation and infiltration of NASICON-type solid electrolytes with microporous channels. *Ceram Int* 2022;48:2203-11. DOI
199. Zhang Z, Wang X, Li X, et al. Review on composite solid electrolytes for solid-state lithium-ion batteries. *Mater Today Sustain* 2023;21:100316. DOI
200. Zheng F, Li C, Li Z, et al. Advanced composite solid electrolytes for lithium batteries: filler dimensional design and ion path optimization. *Small* 2023;19:220655. DOI
201. Liu W, Lee SW, Lin D, et al. Enhancing ionic conductivity in composite polymer electrolytes with well-aligned ceramic nanowires. *Nat Energy* 2017;2:17035. DOI
202. Hua S, Jing MX, Han C, et al. A novel titania nanorods-filled composite solid electrolyte with improved room temperature performance for solid-state Li-ion battery. *Int J Energy Res* 2019;43. DOI
203. Luo B, Wang W, Wang Q, et al. Facilitating ionic conductivity and interfacial stability via oxygen vacancies-enriched TiO_2 micro rods for composite polymer electrolytes. *Chem Eng J* 2023;460:141329. DOI
204. Xu J, Ma G, Wang N, Zhao S, Zhou J. Borderline metal centers on nonporous metal-organic framework nanowire boost fast Li-ion interfacial transport of composite polymer electrolyte. *Small* 2022;18:2204163. DOI
205. Wu Z, Xie Z, Yoshida A, et al. Nickel phosphate nanorod-enhanced polyethylene oxide-based composite polymer electrolytes for solid-state lithium batteries. *J Colloid Interface Sci* 2020;565:110-8. DOI
206. Yu W, Deng N, Shi D, et al. One-dimensional oxide nanostructures possessing reactive surface defects enabled a lithium-rich region and high-voltage stability for all-solid-state composite electrolytes. *ACS Nano* 2023;17:22872-84. DOI
207. Wang L, Yi S, Liu Q, et al. Bifunctional lithium-montmorillonite enabling solid electrolyte with superhigh ionic conductivity for high-performanced lithium metal batteries. *Energy Storage Mater* 2023;63:102961. DOI
208. Xiao Z, Long T, Song L, Zheng Y, Wang C. Research progress of polymer-inorganic filler solid composite electrolyte for lithium-ion batteries. *Ionics* 2021;28:15-26. DOI
209. Zhu L, Zhu P, Fang Q, Jing M, Shen X, Yang L. A novel solid PEO/LLTO-nanowires polymer composite electrolyte for solid-state lithium-ion battery. *Electrochim Acta* 2018;292:718-26. DOI
210. Bi J, Mu D, Wu B, et al. A hybrid solid electrolyte $Li_{0.33}La_{0.557}TiO_3$/poly(acylonitrile) membrane infiltrated with a succinonitrile-based electrolyte for solid state lithium-ion batteries. *J Mater Chem A* 2020;8:706-13. DOI

211. Li Y, Zhang W, Dou Q, Wong KW, Ng KM. $Li_7La_3Zr_2O_{12}$ ceramic nanofiber-incorporated composite polymer electrolytes for lithium metal batteries. *J Mater Chem A* 2019;7:3391-8. DOI
212. Sun J, Li Y, Zhang Q, Hou C, Shi Q, Wang H. A highly ionic conductive poly(methyl methacrylate) composite electrolyte with garnet-typed $Li_{6.75}La_3Zr_{1.75}Nb_{0.25}O_{12}$ nanowires. *Chem Eng J* 2019;375:121922. DOI
213. Ding J, Wang W, Zhang Y, et al. Improving the ionic conductivity of polymer electrolytes induced by ceramic nanowire fillers with abundant lithium vacancies. *Phys Chem Chem Phys* 2024;26:6316-24. DOI
214. Pei X, Mu J, Hong J, Wei W, Luo W, He G. Solution-processed 2D hectorite nanolayers for high-efficient composite solid-state electrolyte. *Appl Clay Sci* 2022;216:106363. DOI
215. Xu M, Xin Z, Wang J, et al. Emerging application of 2D materials for dendrite-free metal batteries. *Energy Mater* 2024;4:400066. DOI
216. Vijayakumar V, Ghosh M, Asokan K, et al. 2D layered nanomaterials as fillers in polymer composite electrolytes for lithium batteries. *Adv Energy Mater* 2023;13:2203326. DOI
217. Liang J, Luo J, Sun Q, Yang X, Li R, Sun X. Recent progress on solid-state hybrid electrolytes for solid-state lithium batteries. *Energy Storage Mater* 2019;21:308-34. DOI
218. Sun Z, Li Y, Zhang S, et al. g-C_3N_4 nanosheets enhanced solid polymer electrolytes with excellent electrochemical performance, mechanical properties, and thermal stability. *J Mater Chem A* 2019;7:11069-76. DOI
219. Wu Q, Fang M, Jiao S, et al. Phase regulation enabling dense polymer-based composite electrolytes for solid-state lithium metal batteries. *Nat Commun* 2023;14:6296. DOI PubMed PMC
220. Xu L, Xiao X, Tu H, et al. Engineering functionalized 2D metal-organic frameworks nanosheets with fast Li^+ conduction for advanced solid Li batteries. *Adv Mater* 2023;35:2303193. DOI
221. Saleem A, Iqbal R, Majeed MK, et al. Boosting lithium-ion conductivity of polymer electrolyte by selective introduction of covalent organic frameworks for safe lithium metal batteries. *Nano Energy* 2024;128:109848. DOI
222. Zhao Y, Li L, Yang H, Fan S, Li S, Tong H. MXene and silk fibroin peptide team up to build a 1+1>2 in situ SEI film. *Energy Storage Mater* 2024;65:103126. DOI
223. Zhao Y, Li L, Zhou D, Shan Y, Chen X, Cui W. A charge equalizer in accordion-MXene-modified layer leading to spherical lithium deposition. *Energy Environ Mater* 2023;6:12463. DOI
224. Shan Y, Li L, Chen X, Fan S, Yang H, Jiang Y. Gentle haulers of lithium-ion-nanomolybdenum carbide fillers in solid polymer electrolyte. *ACS Energy Lett* 2022;7:2289-96. DOI
225. Liu K, Zhang R, Sun J, Wu M, Zhao T. Polyoxyethylene (PEO)|PEO-perovskite|PEO composite electrolyte for all-solid-state lithium metal batteries. *ACS Appl Mater Interfaces* 2019;11:46930-37. DOI PubMed
226. Hamao N, Yamaguchi Y, Hamamoto K. Densification of a NASICON-type LATP electrolyte sheet by a cold-sintering process. *Materials* 2021;14:4737. DOI PubMed PMC
227. Gu B, Zhan C, Liu BH, et al. Two-dimensional layered lithium lanthanum titanium oxide/graphene-like composites as electrodes for lithium-ion batteries. *Dalton Trans* 2022;51:7076-83. DOI
228. Cheng EJ, Liu M, Li Y, Abe T, Kanamura K. Effects of porosity and ionic liquid impregnation on ionic conductivity of garnet-based flexible sheet electrolytes. *J Power Sources* 2022;517:230705. DOI
229. Huang C, Huang S, Wang A, et al. Stabilizing the $Li_{1.4}Al_{0.4}Ti_{1.6}(PO_4)_3$/Li interface with an in situ constructed multifunctional interlayer for high energy density batteries. *J Mater Chem A* 2022;10:25500-8. DOI
230. Liu Z, Borodin A, Endres F. Ionic liquid and polymer coated garnet solid electrolytes for high-energy solid-state lithium metal batteries. *Energy Technol* 2021;10:2100907. DOI
231. Xu K, Xu C, Jiang Y, Cai J, Ni J, Lai C. Sandwich structured PVDF-HFP-based composite solid electrolytes for solid-state lithium metal batteries. *Ionics* 2022;28:3243-53. DOI
232. Fu Y, Gu Z, Gan Q, Mai YW. A review on the ionic conductivity and mechanical properties of composite polymer electrolytes (CPEs) for lithium batteries: insights from the perspective of polymer/filler composites. *Mat Sci Eng R* 2024;160:100815. DOI
233. Jiang T, He P, Liang Y, Fan LZ. All-dry synthesis of self-supporting thin $Li_{10}GeP_2S_{12}$ membrane and interface engineering for solid state lithium metal batteries. *Chem Eng J* 2021;421:129965. DOI
234. Zou S, Yang Y, Wang J, et al. *In situ* polymerization of solid-state polymer electrolytes for lithium metal batteries: a review. *Energy Environ Sci* 2024;17:4426-60. DOI
235. Chen J, Wang C, Wang G, Zhou D, Fan LZ. An interpenetrating network polycarbonate-based composite electrolyte for high-voltage all-solid-state lithium-metal batteries. *Energy Mater* 2022;2:200023. DOI
236. Guo J, Zheng J, Zhang W, Lu Y. Recent advances of composite solid-state electrolytes for lithium-based batteries. *Energy Fuels* 2021;35:11118-40. DOI
237. Xie H, Bao Y, Cheng J, et al. Flexible garnet solid-state electrolyte membranes enabled by Tile-and-Grout design. *ACS Energy Lett* 2019;4:2668-74. DOI
238. Zekoll S, Marriner-Edwards C, Hekselman AKO, et al. Hybrid electrolytes with 3D bicontinuous ordered ceramic and polymer microchannels for all-solid-state batteries. *Energy Environ Sci* 2018;11:185-201. DOI
239. Yang H, Mu D, Wu B, Bi J, Zhang L, Rao S. Improving cathode/$Li_{6.4}La_3Zr_{1.4}Ta_{0.6}O_{12}$ electrolyte interface with a hybrid PVDF-HFP-based buffer layer for solid lithium battery. *J Mater Sci* 2020;55:11451-61. DOI
240. Shen C, Huang Y, Yang J, Chen M, Liu Z. Unraveling the mechanism of ion and electron migration in composite solid-state

electrolyte using conductive atomic force microscopy. *Energy Storage Mater* 2021;39:271-7. DOI

241. Sun M, Liu T, Yuan Y, et al. Visualizing lithium dendrite formation within solid-state electrolytes. *ACS Energy Lett* 2021;6:451-8. DOI
242. Biao J, Han B, Cao Y, et al. Inhibiting formation and reduction of Li_2CO_3 to LiC_x at grain boundaries in garnet electrolytes to prevent Li penetration. *Adv Mater* 2023;35:2208951. DOI
243. Ye Q, Liang H, Wang S, et al. Fabricating a PVDF skin for PEO-based SPE to stabilize the interface both at cathode and anode for Li-ion batteries. *J Energy Chem* 2022;70:356-62. DOI
244. Kozdra S, Wójcik A, Możdżonek M, Florczak Ł, Opaliński I, Michałowski PP. Poly (vinylidene fluoride) solid polymer electrolyte structure revealed by secondary ion mass spectrometry. *Polymer* 2022;259:125364. DOI
245. Li J, Cai Y, Zhang F, et al. Exceptional interfacial conduction and LiF interphase for ultralong life PEO-based all-solid-state batteries. *Nano Energy* 2023;118:108985. DOI
246. Pang P, Bai Y, Wang H, et al. Ga/Ta co-doped LLZO enhanced voltage tolerance and lithium dendrite resistance of composite solid electrolytes. *J Energy Storage* 2024;84:110809. DOI
247. Yang K, Ma J, Li Y, et al. Weak-interaction environment in a composite electrolyte enabling ultralong-cycling high-voltage solid-state lithium batteries. *J Am Chem Soc* 2024;146:11371-81. DOI
248. Li Y, Wang H. Composite solid electrolytes with NASICON-type LATP and PVDF-HFP for solid-state lithium batteries. *Ind Eng Chem Res* 2021;60:1494-500. DOI
249. Wang Z, Chen J, Fu J, Li Z, Guo X. Polymer-based electrolytes for high-voltage solid-state lithium batteries. *Energy Mater* 2024;4:400050. DOI
250. Wang Y, Wu L, Lin Z, et al. Hydrogen bonds enhanced composite polymer electrolyte for high-voltage cathode of solid-state lithium battery. *Nano Energy* 2022;96:107105. DOI
251. Mu Y, Chu Y, Shi Y, et al. Constructing robust LiF-enriched interfaces in high-voltage solid-state lithium batteries utilizing tailored oriented ceramic fiber electrolytes. *Adv Energy Mater* 2024;14:2400725. DOI